Developing a 3D mechanistic model for examining factors contributing to harmful blooms of *Margalefidinium polykrikoides* in a temperate estuary

Qubin Qin[1]*, Jian Shen[1], Kimberly S. Reece[1], Margaret R. Mulholland[2]

[1]Virginia Institute of Marine Science, William & Mary, Gloucester Point, VA 23062, USA

[2]Department of Ocean, Earth and Atmospheric Sciences, Old Dominion University, 4600 Elkhorn Avenue, Norfolk, VA 23529-0276, USA

*Correspondence to:

Qubin Qin

Virginia Institute of Marine Science

William & Mary

Gloucester Point, VA 23062, USA

Email: qubin@vims.edu

Phone: +1 (804) 684-7670

Abstract

Blooms of *Margalefidinium* (previously *Cochlodinium*) *polykrikoides* occur almost annually in summer in the lower Chesapeake Bay and its tributaries (e.g., the James and York Rivers). The Lafayette River, a sub-tributary of the lower James River, has been recognized as an initiation location for blooms in this region. The timing of bloom initiation varies interannually, ranging from late June to early August. To fully understand critical environmental factors controlling bloom initiation and interactions between physical and biological processes, a numerical module simulating *M. polykrikoides* blooms was developed with a focus on the bloom initiation. The module also includes life cycle and behavioral strategies such as mixotrophy, vertical migration, cyst dynamics and grazing suppression. Parameterizations for these behaviors were assigned based on published laboratory culture experiments. The module was coupled with a 3D physical-biogeochemical model for the James River that examined the contribution of each environmental factor and behavioral strategy to bloom initiation and development. Model simulation results highlight the importance of mixotrophy in maintaining high growth rates for *M. polykrikoides* in this region. Model results suggest that while many factors contribute to the initiation process, temperature, physical transport processes, and cyst germination are the three dominant factors controlling the interannual variability in the timing of bloom initiation.

Keywords: *Margalefidinium polykrikoides*; Mixotrophy; Estuary; Physical processes; Cyst germination; Modeling

1. Introduction

Harmful algal blooms (HABs) have been observed in many estuarine and coastal systems, and it has been suggested that anthropogenic nutrient enrichment is contributing to their worldwide expansion (Anderson D.M. et al., 2002; Heisler et al., 2008). *Margalefidinium* (previously *Cochlodinium*) *polykrikoides* is a dinoflagellate HAB species that blooms almost annually in the lower Chesapeake Bay and its tributaries including the James and York Rivers (Marshall 2009; Morse et al., 2013). *M. polykrikoides* blooms observed in the lower Chesapeake Bay appear to initiate at localized "hot spots", and the Lafayette River, a sub-tributary of the lower James River is thought to be one such initiation site (Mulholland et al., 2009; Morse et al., 2011, 2013; Qin and Shen, 2019). Blooms are then transported into adjacent and connected waterways where they can flourish (Morse et al., 2011; 2013). This suggests that the initiation of *M. polykrikoides* blooms is controlled by local conditions affecting cell growth and accumulation.

Margalefidinium polykrikoides blooms typically occur in the summer when warm temperatures are thought to support their growth (Kudela and Gobler, 2012). In the James River, long-term monitoring suggests that the time at which populations reach bloom density (> 1000 cells ml^{-1}, Virginia DEQ, 2019) varies interannually, ranging from late June to early August (Mulholland et al., 2009, 2018; Morse et al., 2011; 2013). In addition, monitoring shows that the duration of *M. polykrikoides* blooms also varies interannually, ranging from several days to several months (Hofmann et al., in review). These fluctuations pose interesting and important questions: How are the bloom dynamics regulated by environmental factors? And, what are the key factors controlling the interannual variability in the timing of *M. polykrikoides* blooms?

Based on daily observational data, Morse et al. (2013) highlighted the important roles of the temperature and localized nutrient inputs from storms for the initiation of the *M. polykrikoides* blooms in the Lafayette River. However, due to the lack of robust local culture isolates and the ephermeral nature of blooms, we still lack a quantitative understanding of many of the factors thought to regulate the growth of *M. polykrikoides* such as their: 1) ecophysiology (e.g., the effects of temperature, salinity, light and nutrient concentrations and their nonlinear interactions); 2) ability to grow mixotrophically; 3) patterns of vertical migration; 4) food-web interactions with other species including grazing suppression and allelopathic effects on competitors; 5) transport processes; and 6) their ability to form temporary and resting cysts to both avoid unfavorable environmental conditions and ensure that there are seed populations available to germinate to vegetative cells when conditions become suitable (e.g., Kudela and Gobler, 2012).

Process-based models with realistic forcings are one of the most powerful tools for quantitifying the relative contributions of various physical and biological factors to bloom formation (Glibert et al., 2010; McGillicuddy, 2010; Anderson C.R. et al., 2015; Franks, 2018). Three dimensional process-based models have been developed and widely used for quantitatively examining biogeochemical processes (e.g., nutrient concentrations, oxygen, algal biomass and productivity) in aquatic systems, but these have been much less used to model HABs. While there are 3D mechanistic models developed for HABs in lakes, estuaries, and coastal marine environments (e.g., McGillicuddy et al., 2005; Gentien et al., 2007; Milroy et al. 2008; Moore et al., 2015; Ralston et al., 2015; Aleynik et al., 2016; Gillibrand et al., 2016; Zhang et al., 2021), the biogeochemical processes in those models are often simplified because it is a challenge to accurately simulate the complex dynamics of HAB species that have multiple

behavioral and adaptive strategies (Anderson C.R. et al., 2015; Ralston et al., 2015; Ralston and Moore, 2020). Nevertheless, these behavioral and life cycle strategies are needed to be suitably simulated in HAB models for improving their modeling skills (Azanza et al., 2018; Flynn and McGillicuddy, 2018; Wells et al., 2020). For example, for harmful mixotrophic species, properly simulating the contribution of mixotrophy to population growth is important (Stoecker et al., 2017; Flynn and McGillicuddy, 2018; Flynn et al., 2018). While approaches for using mathematical models to simulate mixotrophy have been proposed (e.g., Flynn and Mitra, 2009; Mitra and Flynn, 2010; Ghyoot e al., 2017a; Lin et al., 2018) and applied in some biogeochemical models (e.g., Ghyoot et al., 2017b), the explicit modeling of mixotrophy is still rare in large 3D mechanistic HAB models that couple physical and biogeochemical processes. In shallow, estuarine systems, in addition to the construction of equations to describe the processes related to mixotrophy, simulations must include the full nutrient dynamics with nonpoint- and point-source loadings as well as internal nutrient cycles both in the water column and in the bottom sediment.

In this study, a mechanistic model for simulating an *M. polykrikoides* bloom was developed and applied to the lower James River. Values for most model parameters were incorporated from laboratory culture experiments reported in the literature. The developed HAB model was coupled with a 3D hydrodynamic-eutrophication model to fully simulate the dynamics of *M. polykrikoides* under the influence of various estuarine biogeochemical processes. The model was then used to quantitively evaluate the contributions of various environmental factors to the interannual variability in the initiation of *M. polykrikoides* blooms. Environmental factors included: temperature, salinity, light, inorganic nutrient concentrations, bioavailable organic matter and prey, grazing, retention, as well as behavioral strategies such as mixotrophy,

vertical migration, and cyst germination. The terminology used in this study is defined here: 1) "present" refers to the entire period of time when the cell density of *M. polykrikoides* is greater than 0 cell ml^{-1} in the water column, including both bloom and non-bloom periods, 2) "bloom event" refers to the period when cell densities are ≥ 1000 cells ml^{-1}, and 3) "initiation period" is the period when the *M. polykrikoides* cell densities are > 0 but < 1000 cells ml^{-1}.

2. Methods

2.1. Site description

The Lafayette River is a sub-tributary of the lower James River near its confluence with the lower Chesapeake Bay, USA, and is a site where *M. polykrikoides* blooms are thought to initiate (Fig. 1; Mulholland et al., 2009; Morse et al., 2011, 2013; Qin and Shen, 2019). The Lafayette River is a temperate estuary with a mean depth less than 5 m, and its hydrodynamics are largely controlled by tidal forcing (the tidal range is about 1 m), runoff from the urban watershed, and wind. Water temperatures in this estuary vary widely over annual cycles with values in excess of 30°C observed in summer and below 10°C in winter. The primary sources of freshwater to the estuary are rainfall and groundwater, and so in the absence of storms, salinity is primarily controlled by tidal water transport from the lower James River; the average salinity ranges from 15-25. However, when there is heavy rainfall, salinities in the upper Lafayette River can decrease to less than 5.

Monthly environmental data including chlorophyll-a concentrations (chl-a) for 2007-2013 were retrieved from the long-term Chesapeake Bay Program monitoring database (https://www.chesapeakebay.net/) for stations LFB01 and LFA01 in the Lafayette River, and stations LE5.6, and LE5.4 in the Lower James River. An additional station near the mouth of the

Lafayette River at the Norfolk Yacht and Country Club (NYCC) was included in this analysis, it was established as a timeseries site for observing water quality impairments and bloom initiation in 2012. Weekly surface dataflow cruises were conducted by the Hampton Roads Sanitation District in the poly- and mesohaline James River, and in the Elizabeth and Lafayette Rivers to map surface chl-a concentrations between March and October from 2008-2013. During dataflow cruises surface water is pumped through a YSI datasonde equipped with a chl-a sensor. These data are publicly available through the Virginia Estuarine and Coastal Observing System (VECOS, http://web2.vims.edu/vecos/). For model comparison, dataflow chl-a concentrations were spatially averaged over the areas (bounded by the corresponding grid cells) around Stations LFB01, NYCC, LFA01, LE5.6, and LE5.4 to provide the mean values of surface chl-a at the five stations.

Margalefidinium polykrikoides cell abundance in the Lafayette River was quantified using light microscopy (Mulholland et al., 2009; Morse et al., 2011; 2013; 2014; Egerton et al. 2014). Algal cells were identified to the lowest taxonomic unit (usually to the genus or species level) and densities were reported as cells ml^{-1}. Particularly, for better comparing the model output with observational data, we used the data of *M. polykrikoides* cell abundance (cells ml^{-1}) with relatively high frequency (daily) from a station near Station LFB01 in the summer of 2009 (Morse et al. 2013).

2.2. A model for M. polykrikoides blooms in the James River

A HAB module was first developed and built into the James River water quality model (JRWQM). This module is carbon-based and consistent with the 3D hydrodynamic-eutrophication model of Environmental Fluid Dynamics Code (EFDC, Park et al. 1995) used for JRWQM, and the biomass of *M. polykrikoides* was simulated. Cell abundance was calculated

147 from carbon biomass using a conversion factor of 3437 pg C cell^{-1} based on the average cell
148 biovolume for *M. polykrikoides* (Smayda 1978). The results were compared to observational data
149 of *M. polykrikoides* abundance, in units of cells ml^{-1} in 2009. While this module focuses on
150 vegetative cell growth, it includes behavioral and life cycle strategies employed by *M.*
151 *polykrikoides*, such as vertical migration, mixotrophic growth, resting cyst formation, and cyst
152 germination.

153 At a given location, the governing equation for *M. polykrikoides* dynamics can be
154 described as:

$$\frac{\partial C}{\partial t} + u\frac{\partial C}{\partial x} + v\frac{\partial C}{\partial y} + w\frac{\partial C}{\partial z} - \left[\frac{\partial}{\partial x}\left(K_x\frac{\partial C}{\partial x}\right) + \frac{\partial}{\partial y}\left(K_y\frac{\partial C}{\partial y}\right) + \frac{\partial}{\partial z}\left(K_z\frac{\partial C}{\partial z}\right)\right] =$$

155 $$(G - R - M)C + w_c\frac{\partial C}{\partial z} + germ - encyst \qquad (1)$$

156 where C is the density of the HAB species; x, y, z, and t denote the three-dimensional location
157 and time, respectively, of C. The variables u, v, and w are the current velocities in x, y, z
158 dimensions, respectively; and K_x, K_y, K_z are diffusivities in x, y, z dimensions, respectively, G is
159 the gross growth rate, R is the respiration/excretion rate, and M is the mortality rate due to
160 natural death, grazing, and parasitism. w_C denotes the vertical velocity/swimming speed of the
161 algae, *germ* denotes the input rate of vegetative cells from the germination of resting cysts,
162 *encyst* is a sink term denoting the loss rate of vegetative cells due to cyst formation. G is
163 expressed as the product of the optimal gross growth rate and the growth-limiting functions for
164 environmental factors, where each growth-limiting function ranges from 0 (most limiting) to 1
165 (not limiting at all). The details of the module development are described in the Appendix, and
166 the expressions for functions and critical parameters are listed in Table 1.

Detailed descriptions of the JRWQM model, model configuration, and boundary conditions are described in Shen et al. (2016) and Shen and Qin (2019). The formation and germination of temporary cysts can cause significant variability in the density of vegetative cells over diurnal cycles (Shin et al., 2017). The transformation of vegetative cells into temporary cysts is thought to be largely controlled by the light availability (Shin et al., 2017). Because the formation and germination of temporary cysts do not represent a net source or loss term on the time scale of bloom events, rather than adding to the complexity and uncertainty of the module, the current module ignores temporary cyst dynamics.

2.3. Model parameterizations and calibration

The HAB module for *M. polykrikoides* dynamics was applied to examine *M. polykrikoides* blooms in the James River and its tributaries, for which there is a well-calibrated JRWQM model (Shen et al., 2016; Shen and Qin, 2019). The model simulation, with realistic forcings, was conducted from 2006-2013. The year 2006 was used for spinning up the hydrodynamics of the model, and the dynamics of *M. polykrikoides* in the following 7 years (2007-2013) were then simulated. In this study, three algal groups were simulated, *M. polykrikoides* and two non-HAB assemblages, one dominated by diatoms, and the other describing mixed phytoplankton communities including dinoflagellates, chlorophytes, and cryptophytes. Each station was represented by one single grid cell. Statistical analyses were used to evaluate the performance of the model, including the relative error (RE) and the correlation coefficient (r) between the model output and observational chl-a data at the five stations.

Physiological parameterizations in the HAB module were estimated based on culture experiments reported in the literature and adjusted during the calibration process based on both chl-a and cell density data from the lower James River estuary. Model parameterizations used are

listed in Table 2 along with the data sources. As discussed in the Appendix, the mortality rate, M, was set to zero in the model. *M. polykrikoides* is assumed to swim upward when light is limiting during daytime but no swimming activity at night. The swimming speed is set to be w_c = 55 m d^{-1}.

The values for optimal gross growth rates for *M. polykrikoides* were estimated based on the culture experiments conducted by Gobler et al. (2012). They reported maximum specific growth rates of 0.43-0.44 d^{-1} for growth on dissolved inorganic nitrogen (DIN) (>25 µM N) and 0.53 d^{-1} for growth on glutamic acid (>25 µM N) in cultures of *M. polykrikoides* isolated from Long Island, NY, USA, and grown at 21 °C under a 14:10 light:dark cycle. These rates are consistent with those reported for the *M. polykrikoides* Korean ribotype by Kim et al. (2004), 0.41 d^{-1}. These daily growth rates were used to obtain the phototrophic and heterotrophic gross growth rates at the optimal condition (i.e., no limiting at all) and used at each time step in our model experiments that are 1.06 d^{-1} and 0.62 d^{-1}, respectively (Table 2). Heterotrophic growth was assumed to occur under both light and dark conditions. The values of parameters used to compute growth-limiting functions for temperature, $f(T)$, and salinity, $f(Sal)$, were also determined based on experimental results from cultures (Kim et al., 2004; Griffith and Gobler, 2016) using a least-squares fit. The parameter for the effect of light availability on phototrophic growth, G^p, was based on values reported by Kim et al. (2004) and Oh et al. (2006).

Margalefidinium polykrikoides can take up various forms of nitrogen (Mulholland et al., 2009; 2018). Because kinetic experiments demonstrated that the half-saturation coefficients for nitrate and ammonium were similar to each other (Kim et al., 2001; Kudela et al., 2008; Gobler et al., 2012; Hofmann et al., in review), only one half-saturation coefficient for dissolved inorganic nitrogen (DIN) was used. The values of half-saturation coefficients for DIN and

dissolved inorganic phosphorus (DIP) used in the model were 0.028 $g\,N\,m^{-3}$ (2 μM) and 0.0177 $g\,P\,m^{-3}$ (0.57 μM).

For heterotrophic growth, both phagotrophy (grazing on particulate organic matter, POM) and osmotrophy (uptake of dissolved organic matter, DOM) are considered (Appendix). The simulation allows *M. polykrikoides* to graze on POM smaller than 12 μm. This size cutoff is consistent with the size of particles observed to be grazed by the Asian *M. polykrikoides* ribotypes (Jeong et al., 2004; Kudela and Gobler, 2012). The corresponding growth-limiting function for the heterotrophic growth depends on the concentrations of OM_{12}, the bioavailable organic matter (DOM+POM) less than 12 μm in size. By using a Monod-type equation, the half-saturation coefficient for organic matter, OM_{12k}, was estimated to be 0.0263 $g\,C\,m^{-3}$ based on a published culture experiment showing that the growth of *M. polykrikoides* increased with increasing cryptophyte concentration (Jeong et al., 2004). In the lower James River, we assumed that *M. polykrikoides* could not graze on larger co-occurring algae such as *Akashiwo sanguinea* and *Scrippsiella trochoidea* (Morse et al., 2013) due to their size. Because concentrations of cryptophytes in the Lafayette River is generally low in the summer (5-40 cells ml^{-1}, Morse et al., 2013), prey-sized algae are only a small fraction, less than 0.001, of the total biomass of co-occurring algae, *b* (see the definitions in Appendix and Table 2). Simulations used a constant value of 0.001 for the fraction of prey biomass, *b*. According to culture experiments by Jeong et al. (2004), these low prey concentrations would not significantly increase the growth rates of *M. polykrikoides* via phagotrophy. A sensitivity test setting $b = 0$ (i.e., no prey) versus 0.001 showed negligible differences (the detailed comparison is not shown here). The fraction of POM that is bioavailable for *M. polykrikoides* uptake that is not small algae, *a* (see the definitions in Appendix and Table 2) was calibrated by trial and error. Briefly, with a series of *a* increasing in

236 value, we found the value leading to the best match of the model results against observational
237 chl-a data at the five stations (highest *r* and lowest RE). The parameters for respiration (R_0, f^p,
238 and θ_R) were also calibrated (Table 2) and their values are comparable to typical values used in
239 eutrophication or ecosystem models.

240 The condition for initiating the model corresponded to a cyst germination event. The
241 process was simplified as a one-time release of vegetative cells within one day (an initial loading
242 due to germination, $germ_{\text{ini}}$) from the bottom layer over the mesohaline and polyhaline zones of
243 the James River and its tributaries. Sediment samples show that the mean concentration of *M.*
244 *polykrikoides* cysts in wet sediment is 96 cysts g^{-1} in the lower James River (Seaborn and
245 Marshall, 2008). By using the wet sediment density of 2.65 g cm^{-3} and assuming resting cysts in
246 the top 1 cm of the sediment can be germinated and released into the overlying water, the
247 potential concentration of cysts in the sediment is 2.54×10^6 cysts m^{-2}. However, not every cyst
248 can successfully germinate into vegetative cells. Five laboratory experiments by Tang and
249 Gobbler (2012) showed a range of 2-33% and a mean of 12% for the germination rate of *M.*
250 *polykrikoides* cysts in laboratory cultures. It is expected that the germination process in nature
251 may have a lower success rate and therefore, we assumed a germination rate of 1% in the model.
252 This resulted in an estimate of cell loading from cyst germination of about 25,000 cells m^{-2} d^{-1}.
253 The time when cells from cyst germination first enter the water column (referred to as "initial
254 time") was an adjustable parameter, and it is typically that a later initial time corresponds to a
255 later beginning of the bloom; so we were able to calibrate the initial time for each year by trial
256 and error, based on chl-a and cell density data reported in previous studies (Morse et al., 2011,
257 2013; Mulholland et al., 2009). An additional requirement for the germination used for calibrating
258 the initial time is that the water temperature be above 18 °C, consistent with the germination

experiments conducted by Tang and Gobler (2012) (temperatures between 18-21 °C). These temperatures are cooler than those observed during blooms in the lower Chesapeake Bay (Mulholland et al., 2009; 2018).

2.4. Analysis of contributions of each factor

The calibrated model (Base Scenario) was used to analyze the contribution of each environmental factor and behavior strategy to *M. polykrikoides* blooms in the James River and its tributaries, with a focus on bloom initiation. Among all possible behavioral and life cycle strategies of *M. polykrikoides*, the contributions of three, mixotrophic growth, vertical migration, and cyst germination were considered.

For any algal species, the governing equation (1) can be rewritten mathematically into a simplified form:

$$\frac{\partial C}{\partial t} = r_g C \tag{2}$$

The relative growth rate, r_g, represents the net effects of all physical and biological processes on algal dynamics (Qin and Shen, 2017 and 2019). The solution reads:

$$C = C_{ini} exp\left(\int_{t_{ini}}^{t_{bloom}} r_g \, dt\right) \tag{3}$$

where C_{ini} is the initial density at the "initial time" t_{ini}, and t_{bloom} is the day when the bloom density is first reached (i.e., the beginning of the bloom event). Thus, the time required for bloom initiation relative to the time cells are first observed in the water, t_B, is determined by both initial cell density and relative growth rate which can be computed by:

$$t_B = (t_{bloom} - t_{ini}) = \frac{1}{\langle r_g \rangle} \ln(C_{bloom}/C_{ini}) \tag{4}$$

where C_{bloom} is the bloom density, and $\langle r_g \rangle$ is the mean relative growth rate over the initiation period. t_{bloom} is then calculated to be:

$$t_{bloom} = t_{ini} + \frac{1}{\langle r_g \rangle} \ln(C_{bloom}/C_{ini}) \quad (5)$$

In the lower Chesapeake Bay and its tributaries, *M. polykrikoides* is considered to be at bloom density when populations reach 1000 cells ml^{-1} (Virginia DEQ, 2019), the interannual variability in the beginning of an *M. polykrikoides* bloom event is controlled by initial time, t_{ini}, the initial cell density, C_{ini}, and the relative growth rate of vegetative cells over the initiation period, $\langle r_g \rangle$. Eq. (5) suggests that a higher C_{ini}, an earlier t_{ini}, or a higher $\langle r_g \rangle$ can all lead to an earlier start to a bloom.

A variety of environmental factors can potentially change t_{ini}, C_{ini}, and $\langle r_g \rangle$ from year to year and this can contribute to the interannual variability in the start of bloom events, but the relative importance of each factor is different. Cyst germination determines the initial loading of vegetative cells (or the "inoculum") and therefore, the timing of the first appearance of active cells in the water column, so it contributes to the bloom advent, t_{bloom}, by regulating t_{ini} and C_{ini}. In this model study, the initiation of cell growth is set to begin at the time when vegetative cells are first loaded to the water column from the sediment at a rate of 25000 cells m^{-2} d^{-1} ($germ_{ini}$) and this controls C_{ini}. Therefore, because the loading was constant, the contribution of cyst germination to the interannual variability in bloom initiation in Base Scenario is mainly through the variability in the timing of this event, t_{ini}, and can be estimated by comparing the interannual variations in t_{ini} with the variations in the beginning of bloom event. To further investigate the contribution of cyst germination to bloom initiation through C_{ini}, two additional sensitivity tests were conducted in which germination rates, $germ_{ini}$, were increased or

decreased by a factor of 10 (Table 3). Presumably if a larger number of cysts can successfully germinate, a shorter time will be required for bloom initiation.

The contribution of each environmental factor to changes in algal biomass through their impact on relative growth rates $\langle r_g \rangle$ was investigated by examining the depth-integrated algal biomass over the water column using Eq. (1):

$$\frac{\partial B}{\partial t} = (\bar{G} - \bar{R} - \bar{M})B - \overline{F_B}B + germ - encyst \quad (6)$$

where $B = \int_0^H C dz$ is the depth-integrated biomass, z is the vertical location, and H is the water depth. $\bar{G}$ is the vertical mean gross growth rate that accounts for the growth of B, and $\bar{G} = \frac{\int_0^H (GC) dz}{B}$, $\overline{F_B}$ is the transport rate accounting for the effect of physical transport processes, which is expressed as:

$$\overline{F_B} = \frac{1}{B}\int_0^H \left[u\frac{\partial C}{\partial x} + v\frac{\partial C}{\partial y} + w\frac{\partial C}{\partial z} - \frac{\partial}{\partial x}\left(K\frac{\partial C}{\partial x}\right) - \frac{\partial}{\partial y}\left(K\frac{\partial C}{\partial y}\right) - \frac{\partial}{\partial z}\left(K\frac{\partial C}{\partial z}\right)\right] dz \quad (7)$$

$\overline{F_B}$ at the given location describes the horizontal transport in or out of the estuary, a positive $\overline{F_B}$ suggests that there is net transport out of the estuary that decreases local algal density while a negative $\overline{F_B}$ corresponds to a net transport in to the estuary that increases local algal density (Qin and Shen, 2019; 2021). Note that the integration of the vertical migration/swimming term in Eq. (1), $\int_0^H w_c \frac{\partial C}{\partial z} dz$, equals zero. Because the numerical experiments conducted here used a one-time cyst germination event lasting one day to generate an initial loading of vegetative cells (i.e., initial condition *germ* = $germ_{ini}$), it does not explicitly consider additional cell inputs from germination over a longer time period and cell losses due to cyst formation; therefore, both *germ* and *encyst* are zero after the initial release. Without considering losses from grazing mortality

(i.e., M = 0), the rate equation for depth-integrated *M. polykrikoides* growth can be obtained by dividing by B on both sides of Eq. (6):

$$\overline{r_g} = \bar{G} - \bar{R} - \overline{F_B} \quad (8)$$

where $\overline{r_g} = \frac{\partial B}{B \partial t}$ is relative growth rate for the depth-integrated biomass and $\langle \bar{G} \rangle$, $\langle \bar{R} \rangle$, and $\langle \overline{F_B} \rangle$ are the mean values of growth, respiration, and physical transport, respectively, over the time increment examined (i.e., "Present Period", "Initiation Period"). With the numerical model, the relative contribution of each term in Eq. (8) was examined by comparing their values over each period when *M. polykrikoides* was present and during its initiation period. Particularly, $\langle \overline{F_B} \rangle$ was computed from the balance of the remaining terms. As shown by Eq. (8), for successful bloom initiation, $\langle \overline{F_B} \rangle$ must be less than the net growth rate of *M. polykrikoides*, $\langle \bar{G} \rangle - \langle \bar{R} \rangle$, during the initiation period. Since $\overline{G^p}$ and $\overline{G^h}$ are also computed in the model, the mean phototrophic growth rate $\langle \overline{G^p} \rangle$ and mean heterotrophic growth rate $\langle \overline{G^h} \rangle$ were also computed. $\langle \overline{G^h} \rangle$ was compared to $\langle \bar{G} \rangle$ to examine the importance of mixotrophic growth for initiating and developing *M. polykrikoides* blooms. Additional numerical experiments were conducted to investigate the model sensitivities to fractions of bioavailable particulate organic matter and mixotrophic capability (Table 3). Sensitivity tests were also conducted for evaluating swimming speed in contributing to bloom development.

Since the interannual variability in bloom initiation is regulated by that in $\langle \overline{r_g} \rangle$, which terms in Eq. (8) contributed most to the 7-year interannual variability in $\langle \overline{r_g} \rangle$ was evaluated statistically by calculating and comparing the standard deviations of $\langle \overline{r_g} \rangle$, $\langle \bar{G} \rangle$, $\langle \bar{R} \rangle$, and $\langle \overline{F_B} \rangle$ during initiation periods.

342 The major contributions of environmental factors to the initiation and development of *M.*
343 *polykrikoides* blooms were also examined using the model. Note that the contribution of each
344 factor to bloom initiation is different from their contributions to the interannual variability in the
345 timing of bloom initiation. A factor may be important in supporting algal growth during bloom
346 initiation without being important in regulating the timing of bloom initiation because there is
347 interannual variability in most environmental factors. For temperature, salinity, light, *DIN*, *DIP*,
348 and bioavailable organic matter, growth-limiting functions that regulate the gross growth rate of
349 *M. polykrikoides* were compared with each other to examine which factor limited algal growth.
350 To examine the contribution of temperature and salinity to the interannual variability in the time
351 when bloom cell densities were reached, we calculated the coefficient of determination (r^2)
352 between the mean of the gross growth rate (G) during each initiation period (7 events over 7
353 years) and the mean of the growth-limiting functions ($f(T)f(Sal)$) for each of the two factors.
354 For the resources (light, inorganic nutrients, and bioavailable organic matter), as shown in
355 Appendix Eqs. (A1) (A2) and (A3), their effects on the growth rate, G, interact with each other.
356 By using a function f (Res) describing the interaction effect of these resources makes $G =$
357 $G_{opt}f(T)f(Sal)f(Res)$, the total contribution of resources to the interannual variability in the
358 beginning of the bloom was examined by comparing r^2 between f (Res) and G. Values of f (Res)
359 were directly output by the model. The contribution of each resource to G was weighted by its
360 significance in the total contribution, which was indicated by r^2 between f (Res) and growth-
361 limiting function for each resource. The contribution of each factor to the intra-annual variability
362 in the growth was also examined by computing r^2 between G and the growth-limiting functions
363 for temperature, salinity, and the resource combination on daily timescales. The above analyses

were done for both the periods of bloom initiation and the periods when *M. polykrikoides* was present (including both bloom and non-bloom periods).

3. Results

3.1. Model simulation results

Model results agree reasonably well with the observed chl-a concentrations at the five long-term monitoring stations, for which there are monthly observations, and weekly dataflow data for the Lafayette, Elizabeth and lower James Rivers (Fig. 2). The correlation coefficients, *r*, ranged from 0.56-0.90 and relative errors, RE, ranged from 0.25-0.36, indicating that the model reasonably simulated the variability in *M. polykrikoides* cell density during each bloom year and the interannual variability in the timing and magnitude of *M. polykrikoides* blooms in the lower James River and its tributaries. When *M. polykrikoides* was not included in the model (i.e., only the two non-HAB species were simulated), the summer *M. polykrikoides* bloom did not occur within the model simulation period (Supplementary Fig. S1). There was good agreement between simulated and observed *M. polykrikoides* cell densities in the Lafayette River under the Base Scenario in 2009 (Fig. 3), considering the large variations among observations. The model results also reproduced the interannual variability in the timing of bloom initiation (Table 4). The bloom occurred as early as late June in 2009 and 2012, but did not develop until late July or even early August in the other 5 study years.

There were also some discrepancies between the observations and the model results. In the years when the bloom was first observed in late July or early August, the model shows a second bloom and overestimates algal density (e.g., 2008, 2010, and 2011) while observations do not corroborate this. Observations show that once bloom events were terminated, they generally

386 did not return. This suggests that the model is lacking some factors or mechanisms for bloom
387 termination. Statistics show there is generally higher *r* and lower RE between the model results
388 and observations if the termination periods are not included, indicating that the model performed
389 better for algal dynamics during initiation periods.

390 ### *3.2. Interannual variability in t_{ini}, $\langle r_g \rangle$, and t_{bloom}*

391 The importance of the effect of variance in t_{ini} and $\langle r_g \rangle$ on the interannual variability in
392 the start of the bloom, t_{bloom}, was evaluated using the model. Over the 7 years, t_{ini} varied from
393 April 15th to July 1st with a range of 77 d (Table 4), suggesting that the variations in t_{ini}
394 contributed disproportionately to the timing of bloom initiation. Variations in $\langle r_g \rangle$ during the
395 bloom initiation periods also showed large interannual shifts, and $\langle \overline{r_g} \rangle$ ranged from 0.24 to 1.08
396 d^{-1} at LFB01 (Table S1). The difference in $\langle r_g \rangle$ suggests that each year *M. polykrikoides*
397 experienced very different environmental conditions during initiation periods, which contributed
398 to the interannual variability in the length of the initiation period, t_B. At LFB01, t_B varied from
399 17 to 69 d over the 7-year study period. The variability in t_{ini} and that in t_B resulted in the large
400 interannual variability in the beginning of the bloom event, t_{bloom}, which varied from June 22 in
401 2012 to July 24 in 2011 with a range of 32 d at Station LFB01 (Table 4).

402 ### *3.3. Standard deviations of $\langle \overline{r_g} \rangle$, $\langle \bar{G} \rangle$, $\langle \bar{R} \rangle$, and $\langle \overline{F_B} \rangle$*

403 During initiation periods, at the three stations (LFB01, NYCC, LFA01) in the Lafayette
404 River, the standard deviations for $\langle \overline{r_g} \rangle$ were 0.29 d^{-1}, 0.16 d^{-1}, and 0.10 d^{-1}, respectively, for $\langle \overline{F_B} \rangle$
405 they were 0.34 d^{-1}, 0.18 d^{-1}, and 0.09 d^{-1}, respectively; and for $\langle \bar{G} \rangle$ they were 0.11 d^{-1}, 0.08 d^{-1},
406 and 0.07 d^{-1}, respectively. The standard deviations in $\langle \overline{F_B} \rangle$ and $\langle \bar{G} \rangle$ were much larger than those

for respiration rates, $\langle \bar{R} \rangle$ (< 0.01 d^{-1} at the three stations); this demonstrates that flushing and factors affecting growth rates determined the interannual variability in $\langle \overline{r_g} \rangle$.

3.4. Contribution of behavioral strategies to bloom

The impacts of the three behavioral and life cycle strategies considered here (mixotrophic growth, swimming, and cyst germination) were examined using Base Scenario and sensitivity experiments. Model results in Base Scenario show that the overall contribution of heterotrophy to growth rates of *M. polykrikoides*, $\bar{G}$, were about 0.18, 0.27, 0.30, 0.30, and 0.34 d^{-1}, at the stations in the Lafayette (LFB01, NYCC, and LFA01), the Elizabeth (LE5.6), and the lower James (LE5.4), respectively (Table 5). $\bar{G}$ during the initiation periods in the model were much higher, with about 0.31, 0.40, 0.42, 0.44, 0.48 d^{-1}, respectively, at the five stations. Heterotrophic growth (osmotrophic + phagotrophic) was found to be as important as phototrophic growth, and $\overline{G^h}$ accounted for about 42-63% of the total growth, $\bar{G}$, when *M. polykrikoides* was present and about 44-61% during the bloom initiation period over the 7 model years at the five stations. When the heterotrophic growth rate was set to zero, i.e., *M. polykrikoides* growth was strictly autotrophic, results showed that *M. polykrikoides* blooms were reduced in magnitude and their initiation was delayed in 2008-2010 and suppressed entirely in other model years in the Lafayette River. Further, even if they initiated, blooms did not propagate throughout the Elizabeth and the lower James Rivers if the heterotrophic subsidy was not allowed (Fig. S2). This indicates that mixotrophic growth is essential for blooms in this region to initiate, develop and proliferate. Results suggest that both phagotrophy and osmotrophy contributed to the bloom magnitude and duration. The observation-derived *b* of 0.001 and the calibrated *a* of 0.01 (see the definition in Appendix and Table 2) suggest that only a very low fraction of living algae and other POM in the water were bioavailable for phagotrophic growth. When there was a higher percentage of

bioavailable POM, e.g., a = 0.1 (Exp. 1), cell abundances of *M. polykrikoides* were higher than the Base Scenario during the bloom events (Fig. 4A). On the other hand, in simulations where heterotrophic growth of *M. polykrikoides* was only through osmotrophy (Exp. 2) (i.e., $a = b = 0$), *M. polykrikoides* blooms were comparable to Base Scenario, with cell abundances slightly smaller in magnitude, suggesting that osmotrophy is the quantitatively more important than phagotrophy to the development of blooms. In Exp. 1 when there was a higher fraction of bioavailable POM (a = 0.1) and in Exp. 2 in which only osmotrophy was allowed ($a = b = 0$), the timing of *M. polykrikoides* achieving bloom concentrations shifted only slightly (by 0-1.3 d) across years (Table 6), except for 2011 at LFA01. In 2011, modeled cell abundance at LFA01 first reached bloom densities (1000 cells ml^{-1}) on Aug. 8 but was very close to the bloom density on July 23 in Base Scenario (Fig. S3B). This shift in timing was due to the higher bioavailable POM in Exp. 1 relative to the Base Scenario, which made the density on July 23 have reached the bloom density and shifted the beginning of the bloom event more than 15 d earlier. This large shift was not observed at LFB01 since cell abundance there was over the bloom density on July 24 in both Base Scenario and Exp. 1 (Fig. S3A).

When swimming speed was reduced, bloom timing (Table 6) and magnitude (Fig. 4B) changed significantly. As shown above, the large interannual variation in t_{ini} in Base Scenario suggests that the timing of cyst germination contributed largely to the interannual variability in the start of the bloom event. In addition, a 10-fold increase or decrease in the initial loading of vegetative cells, $germ_{\mathrm{ini}}$, did not cause a large change in the overall magnitude of blooms after the blooms initiated (Fig. 4C), but changes in cell loading did impact the timing of bloom initiation (Table 6), suggesting the importance of the cyst abundance and the success of cyst germination. However, the magnitude of the shift in bloom initiation varied interannually. For

example, with a 10-fold increase in cyst germination the start of the bloom event at LFB01 in 2007 advanced by 2.0 d but in 2009 it advanced by 13 d.

3.5. Contribution of environmental factors to blooms

Because the model assumes that *M. polykrikoides* are not grazed, the main factors contributing to the dynamics of *M. polykrikoides* blooms were primarily through growth and transport. In general, during the period when *M. polykrikoides* was present in the water column the growth-limiting function for temperature, f (T), and for salinity, f (Sal), were about 0.59-0.87 and about 0.48-0.61 over the region, respectively (Table 7). The average value of f (*Sal*) was generally lower than f (*T*). The average value of growth-limiting function for light, f (I), was about 0.97 during the daytime in the surface layer, suggesting that light did not limit phototrophic growth of *M. polykrikoides*. Both DIP and DIN can be limiting factors for phototrophic growth of phytoplankton in estuaries. Model results suggest that DIN limitation, in general, was often the dominant limiting nutrient at station LFB01 in the upper Lafayette River during intense blooms (Fig. 5), while DIP was the dominant limiting factor near the mouth of the Lafayette (e.g., LFA01) and in the lower Elizabeth and the lower James Rivers. Bioavailable organic matter was less limiting than either DIN or DIP in this region during simulated blooms, especially during the initiation periods, when the function for bioavailable organic matter, f (OM_{12}), had the values over 0.9. f (OM_{12}). However, bioavailable organic matter dropped to a lower value during intense blooms (e.g., Figs. 5E and 5F). During those periods, nutrients became severely limiting for both phototrophic and heterotrophic growth, and the gross growth rate, G, was significantly lower than G_{TS}.

Among all the factors considered, temperature was the dominant factor driving both the interannual and intra-annual variability in gross growth rates, G, in the region (Table 8). Overall,

476 f (T) explained 67-75% of the interannual variability and 40-42% of the daily variability in G
477 during periods when *M. polykrikoides* was present in the water column at the Lafayette River
478 stations (LFB01, NYCC, and LFA01); and explained 61-95% of the interannual variability and
479 82-94% of the daily variability in G during bloom initiation. Temperature regulates the
480 interannual variability through both phototrophic and heterotrophic growths. As shown in
481 Appendix Eqs. (A1) and (A2), both growth rates are a function of temperature. For example, at
482 Station LFB01, the correlation between f (T) and G is 0.67 for interannual variability for the
483 present period, and the corresponding correlations between f (T) and G^p and f (T) and G^h are
484 0.67 and 0.58, respectively. The correlation between f (T) and G is 0.95 for interannual
485 variability for the initiation period, and the corresponding correlations between f (T) and G^p and
486 f (T) and G^h are 0.94 and 0.72, respectively. Other factors (light and nutrients), indicated by the
487 large values of f (Res), contributed less than temperature. In the lower Elizabeth River (LE5.6)
488 and the lower James River (LE5.4), resources contributed less than temperature to the
489 interannual variability in G but was as important as temperature to the intra-annual variabilities
490 in G.

491 In addition to local factors affecting their growth, physical transport played a critical role
492 in controlling *M. polykrikoides* cell density during blooms. The effects of transport were
493 examined by including a function for transport rates, $\overline{F_B}$, which had mean values of up to 0.10 d^{-1}
494 during periods when *M. polykrikoides* was present in the water column and -0.15 to 0.14 d^{-1}
495 during the bloom initiation periods at the five stations (Table 5). These values are not trivial
496 compared to the mean gross growth rates, $\bar{G}$. The absolute values of mean $\overline{F_B}/\bar{G}$ were about 6-29%
497 during the periods when *M. polykrikoides* was present and 5-48% during bloom initiation. In
498 different years, $\overline{F_B}$ was both positive and negative (Table S1), demonstrating that cell

abundances were controlled both by net "transport-in" and "transport-out" processes. During the initiation periods, Stations LFB01 and NYCC show overall net "transport in" (Table 5). Over multiple years these two stations more frequently "transported-in" (negative $\overline{F_B}$) cells than they "transported-out" (positive $\overline{F_B}$) cells (Table S1) (i.e., a net transport of cells into the area around the stations). All the other three stations had positive values of $\overline{F_B}$ for most years, indicating cells there experienced "transport-out" processes more frequently.

4. Discussion

4.1. The importance of mixotrophy

Mixotrophy has now been shown to be common among dinoflagellates (Burkholder et al., 2008; Joeng et al., 2015; Stoecker et al., 2017; Flynn et al., 2018), including the HAB species *M. polykrikoides* (Joeng et al., 2004; Mulholland et al., 2009), and that there are different types of mixotrophy among algal species (Jones, 1997; Stoecker, 1998; Mitra et al., 2016). For *M. polykrikoides*, it is still unclear whether phototrophic or heterotrophic growth is preferred. In the current model, *M. polykrikoides* is assumed to favor phototrophic growth, and heterotrophic growth is performed to complement the total growth (Appendix Eq. A4). This parameterization leads to a minimum amount of nutrient acquisition from heterotrophy. We also tested in the model *M. polykrikoides* performing phototrophic and heterotrophic growth simultaneously, i.e., no preference on the growth mode (Appendix Eq. A5) and the model results showed that the contribution of heterotrophic growth was about 7-10% higher than Base Scenario when phototrophic growth was favored over the entire period when *M. polykrikoides* is present in the water column and about 9-14% higher for the bloom initiation periods (Data not shown). This

indicates that the ability to employ heterotrophy to augment autotrophy is an important adaptive strategy that promotes blooms of this organism.

Our model results show that heterotrophy contributes significantly to the growth of *M. polykrikoides* in the lower Chesapeake Bay region. This is supported by model results showing $f(\mathrm{OM}_{12})$ above 0.70 in surface water during blooms (Table 7). During bloom initiation, bioavailable organic matter was even more abundant with $f(\mathrm{OM}_{12})$ found to be over 0.90. Correspondingly, the model results of $\langle\overline{G^h}\rangle/\langle\bar{G}\rangle$ suggest that heterotrophic growth contributed about half to the total growth rate of *M. polykrikoides* (Table 5). Note that uncertainties exist in the model results, as the values of many parameters used in the model (e.g., gross growth rates, swimming speed/vertical migration) are derived from laboratory measurements (Table 2) using cultured isolates from other parts of the world where environmental conditions differ from those observed in the lower Chesapeake Bay region. For example, across much of the globe, *M. polykrikoides* blooms at higher salinities and lower temperatures than those found in the Chesapeake Bay (Kudela and Gobler, 2012; Mulholland et al., 2018). Nevertheless, the model results are reasonable and consistent with field observations where dissolved inorganic carbon accounted for only a small fraction of the total carbon uptake during both bloom and non-bloom periods in the Lafayette and Elizabeth Rivers (Mulholland et al. 2009, 2018). According to the model, uptake of DOM via osmotrophy can support the heterotrophic growth of *M. polykrikoides* and result in high cell densities blooms. The model calibration shows that bioavailable POM only accounted for a very low fraction of the POM in the water column. If the fraction of bioavailable POM were higher, results from Exp. 1 suggest that bloom cell densities would be higher. But *M. polykrikoides* prey, e.g., cryptophytes, were not abundant during blooms (Morse et al., 2013).

It should be noted that among the environmental factors regulating growth rate, the uncertainty in heterotrophic growth may come from estimated nutrient concentrations. Overall this has a limited effect that heterotrophy has on the total mixotrophic growth and the contribution to a relatively high growth rate. Although the swimming behavior in the model may also alter the heterotrophic growth due to changes in nutrient and flushing conditions at different vertical locations, the overall ratio of dissolved inorganic nutrients to bioavailable organic nutrients does not vary largely in the study region. Therefore, the uncertainty caused by the choice of swimming behavior or speed will not change the important role of mixotrophy. This is demonstrated in the two swimming experiments. $\langle \overline{G^h} \rangle / \langle \bar{G} \rangle$ at Station LFB01 are 0.56 and 0.61, respectively, for the present period in Exp. 4 (reduced swimming speed) and Exp. 5 (no swimming). These values are not largely different from the Base Scenario, 0.51 (Table 5). The other stations also show similar results. This suggests that mixotrophy consistently plays a central role in *M. polykrikoides* blooms with varying swimming speed.

4.2. Dominant Factors controlling the interannual variability in the start of bloom events

Many factors contribute to bloom initiation (Morse et al., 2013), and model results and observations suggest that the length of time required for blooms to initiate varies substantially from year to year. In the model framework, the interannual variability in time *M. polykrikoides* cells reach bloom density, t_{bloom}, is affected by cyst germination and by variations in environmental factors that can regulate growth and by variations in physical transport.

4.2.1. Cyst germination

Margalefidinium polykrikoides produce resting cysts and cyst production and germination are thought to contribute the near-annual recurrence of blooms and their initiation in

566 estuaries and coasts (Kudela and Gobler, 2012; Tang and Gobler, 2012). In the lower James
567 River and its tributaries, model results suggest that the timing and relative success of cyst
568 germination may contribute substantially to the interannual variability in the start of bloom
569 events, t_{bloom}, by determining t_{ini} and C_{ini} in Eq. (5). It is worth noting that the cyst
570 germination process for *M. polykrikoides* may also be temperature dependent, and this may
571 affect the interannual variability in t_{ini}. Tang and Gobbler (2012) showed that cyst germination
572 occurred over a shorter time period in the lab when it was cultured at a higher temperature.
573 Temperature may also impact on t_{ini} through other mechanisms such as the cyst chilling concept
574 (Fischer et al., 2018). The model does not consider this or the loss of vegetative cells due to
575 resting cyst formation during bloom initiation periods because cyst formation is to be minor until
576 populations reach high cell densities in late exponential or stationary phase of growth (Garcés et
577 al., 2004; Tang and Gobler, 2012; Brosnahan et al., 2017).

578 4.2.2. Temperature and salinity

579 As highlighted in Appendix Eqs. (A1) and (A2), temperature and salinity were two
580 factors regulating phototrophic and heterotrophic growth rates in the model. Previous studies
581 have shown that temperature plays an important role in the timing of blooms of *M. polykrikoides*
582 in the lower James River and its tributaries (Mulholland et al., 2009, 2018) as well as in other
583 systems (Kudela and Gobler, 2012). Culture studies using a Long Island isolate suggest that *M.*
584 *polykrikoides* grows optimally at temperatures ranging from 21-26 ^{o}C and salinities between 30
585 and 36 although Korean ribotypes grow at temperatures ranging from 15-30 ^{o}C and salinities
586 between 20-36 (Kim et al., 2004). Salinities are characteristically at the lower end and
587 temperatures at the higher end of these ranges in the lower James River estuary and the Lafayette
588 River (Morse et al., 2011, 2013, 2014; Mulholland et al., 2009, 2018). Model results show that

589 temperature is not a severe limiting factor during the initiation period in the Lafayette River but
590 it is the most important factor regulating both the intra-annual and interannual variabilities in
591 gross growth rates, G. The generally lower values of *f* (*Sal*) than *f* (*T*) suggest that the growth of
592 *M. polykrikoides* is more limited by salinity than temperature; but the role of salinity in driving
593 the interannual variability in the initiation of blooms events is far less important compared to
594 temperature, because the salinity typically varies less across years than the temperature in the
595 region.

596 4.2.3. Light, dissolved inorganic nutrients, and bioavailable organic matter

597 The gross growth rate, *G*, was not limited by light although light attenuation is generally
598 rapid during summer in this region (1% light level ranges from 2-3 m in depth; Echevarria et al.
599 unpublished data). The pattern of vertical migration of *M. polykrikoides*, however, suggests that
600 cells stay near the surface during daytime (Morse et al., 2013; Echevarria et al. unpublished data)
601 where they receive abundant light for growth, and migrate to the bottom at night where they can
602 evade predation or access nutrients present in bottom waters. This is supported by the model
603 result showing that *f* (I) was over 0.97 at the three Lafayette River Stations.

604 In contrast, model simulations showed that concentrations of DIN and DIP limited
605 photoautotrophic growth of *M. polykrikoides* during the bloom initiation period. Model
606 simulations showed that the concentrations of DIN and DIP were low relative to half-saturation
607 constants for DIN (2-3 μM) and DIP (0.57 μM) during blooms (Gobler et al., 2012; Kim et al.,
608 2001). Based on the model results and observed DIN and DIP concentrations in the James and
609 Lafayette Rivers (Filippino et al., 2017; Morse et al., 2011, 2013, 2014; Mulholland et al., 2009,
610 2018), the supply of DIN may limit photoautotrophic growth by *M. polykrikoides* in the most
611 areas of the Lafayette during bloom initiation periods. Indeed, the model results show the

612 average value of growth-limiting function for DIN, *f* (DIN), was lower than that for DIP, *f* (DIP),
613 at LFB01 (Table 7). However, the model suggests that DIP is more limiting than DIN at LFA01,
614 a location near the mouth of the estuary where the loading of nutrients is largely influenced by
615 the water exchange between the mainstem James and the tributaries. The half-saturation
616 coefficient, P_k, used for the model was from a culture experiment reported in Kim et al. (2001)
617 for the Korean *M. polykrikoides* ribotype, and if the P_k for the local ribotype was lower,
618 phosphate limitation would be alleviated. In addition, bioavailable organic matter, which could
619 include nitrogen and phosphorus, was relatively abundant and contributed substantially to the
620 initiation process by supporting high mixotrophic growth rates. Analyses of model results show
621 that although these resources (light and nutrients) contributed greatly to the magnitude of G
622 during bloom initiation, their total contribution to the interannual variability in G or t_{bloom} was
623 not as important as temperature, suggested by the lower r^2 between G and the growth-limiting
624 functions for resources, *f* (*Res*) (Table 8). In addition, the above analysis of resource
625 contributions indicates that mixotrophy is not as essential as temperature in regulating the
626 interannual variability of G or t_{bloom}. This is because heterotrophic growth is determined by
627 bioavailable organic matter, which is relatively abundant and *f* (OM_{12}) varies little during
628 initiation periods from year to year (Table S2).

629 4.2.4. Flushing by physical transport

630 Successful bloom initiation requires a positive mean relative growth rate (Qin and Shen,
631 2019), and flushing regulates cell transport and residence time and determines whether cells can
632 accumulate and proliferate or whether they are "washed out" (Anderson D.M. and Stolzenbach,
633 1985; Ralston et al., 2015; Filippino et al., 2017; Phlips et al., 2020). A large transport away
634 from initiation sites can delay initiation of *M. polykrikoides* blooms by reducing biomass

accumulation (Qin and Shen, 2019). At high flow rates, *M. polykrikoides* are transported out of the estuary at greater rates than they can reproduce thereby preventing the accumulation of cell biomass (Morse et al., 2013; Filippino et al., 2017). The large variability in transport rates during the period when bloom initiation is favored suggests that transport processes can significantly contribute to the interannual variability in the length of the initiation period and the time at which bloom cell densities are achieved. The standard deviations in $\langle\overline{F_B}\rangle$ during initiation periods are comparable to or even larger than those for gross growth rates, $\langle\bar{G}\rangle$. Consequently, transport processes are an important regulator of interannual variability in the timing of the start of bloom events, t_{bloom}.

As shown by the expression of F_B (Eq. 7), the flushing effects are determined by external physical forcings through the hydrodynamic field and spatial gradients of algal density (Qin and Shen, 2021). Since a successful initiation of *M. polykrikoides* bloom requires at least several weeks, which is regulated mainly by the estuarine circulation and spring-neap tidal cycles. The major physical forcings driving estuarine circulation include freshwater discharge, wind, and tide. In the Lafayette River, the freshwater discharge is mainly caused by precipitation. Large runoff induced by heavy precipitation or even storms can greatly increase flushing (e.g., Filippino et al., 2017). Wind can alter horizontal transport in this area. Hong et al. (2018) showed that the southerly wind increases the exchange between the lower James River and Elizabeth River and enhances the transport of dissolved substances to the James River, whilst the northerly wind reduces the exchange and inhibits the transport. On the subtidal timescale, spring tide may also increase the exchange flow at the mouth of the Lafayette River and lead to an enhanced transport-out effect.

The spatial gradients of algal density are mainly due to the spatial variability in the local biological growth of *M. polykrikoides* under environmental conditions (temperature, salinity, nutrients, and others). For a location, $F_B > 0$ if the incoming water has a lower density, and $F_B < 0$ if the incoming water has a higher density (Qin and Shen, 2019; 2021).

4.2.5. Vertical migration and stratification

Vertical migration, thought to be regulated by environmental conditions such as light (Smayda, 2002), allows algal species to change their vertical position in the water column and is common among dinoflagellates including *M. polykrikoides* (Sohn et al., 2011; Lim et al., 2014; Jeong et al. 2015). Vertical migration can be beneficial for algae in many ways, including facilitating their acquisition of nutrient resources and avoiding grazers (Jeong et al., 2015). Migration of cells to the surface during daytime helps *M. polykrikoides* acquire light and alleviate light limitation during the day (Morse et al., 2013); correspondingly, model results show that the daily-averaged growth-limiting function for light, *f* (I), was above 0.97.

Margalefidinium polykrikoides is the fastest phototrophic dinoflagellate with the maximum swimming speed of about 1449 μm s^{-1} (Jeong et al., 1999; Jeong et al., 2015), so it may only take them a few hours to migrate vertically from the bottom to the surface in the shallow tidal system. Due to the superior swimming ability of *M. polykrikoides* and the shallow depth of this tidal system, the impact of stratification on the settling of cells is also likely to be unimportant.

Another effect of vertical migration on blooms is through its interaction with physical transport (Anderson D.M. and Stolzenbach, 1985). Ralston et al. (2015) showed that different swimming behaviors of mobile algae can alter the hydrodynamic forcing they encounter and affect the retention of cells. Swimming speed can affect the vertical position of cells in the water

column and therefore the hydrodynamic forces and environmental conditions encountered. This affects both the growing environments and flushing conditions for *M. polykrikoides*. Thus, the nonlinear interaction between *M. polykrikoides* swimming speed, vertical position in the water column, and the hydrodynamics can impact the algal growth and accumulation. The sensitivity of the model to the swimming speed (Table 6 and Fig. 4B) suggests that it plays an important role in regulating bloom initiation; different swimming speeds led to significantly different trajectories for *M. polykrikoides* blooms in the model. Because a constant swimming speed was applied over the years, swimming speed did not contribute substantially to the interannual variability in the initiation of blooms in the current model framework. The variability in swimming speeds in natural systems warrant further examination.

While many factors can contribute to the initiation of *M. polykrikoides* bloom events in the Lafayette River, cyst germination and two environmental factors (temperature and estuarine transport processes/flushing) are key factors contributing to the interannual variability in t_{bloom}. The other environmental factors (salinity, light, dissolved inorganic nutrients) and nutrient acquisition strategies (mixotrophy and swimming) may be less important in affecting the timing of the start of the bloom, t_{bloom}, due to their small interannual variations, however they can affect the length of bloom initiation.

4.3. Model limitation and future work

The model developed performs reasonably well in simulating the initiation of *M. polykrikoides* blooms in the Lafayette River, and it was useful for improving our understanding of how metabolic and behavioral strategies employed by *M. polykrikoides* contribute to bloom initiation and development. However, the results of simulations show some discrepancies with field observations. The inconsistencies between model results and observational data potentially

arose from a variety of sources. First, the model resolution (several hundred meters) may not be fine enough to properly simulate the local patchiness in chl-a concentrations in the small tributary. Because the model focuses on *M. polykrikoides* blooms originating locally within the James River and its tributaries, bloom development outside of the James River was not considered. Second, uncertainties exist in the applicability of values of physiological parameters used as model input. Many parameterizations are from laboratory measurements (e.g., gross growth rate, half-saturation for nutrients, the constant C:Chl, swimming speed, and the conversion from density units to carbon units) using cultured isolates from Korea or Long Island, NY where environmental, and thus culture, conditions are dissimilar to those found where *M. polykrikoides* blooms in the lower Chesapeake Bay watershed. Third, the current structure of the model may introduce biases in the simulation, both for *M. polykrikoides* and for other algal assemblages. For example, only the dynamics of *M. polykrikoides* is modeled explicitly as a water-quality state variable, other algal species are lumped into two assemblages simulated by two state variables. Field observations conducted by Morse et al. (2013) indicate that the dinoflagellates *Gymnodinium uncatenum*, *Scrippsiella trochoidea*, and *Akashiwo sanguinea* were present in high abundance during the *M. polykrikoides* bloom initiation period in 2009. There are commonly blooms of multiple dinoflagellate species during summer in the lower Chesapeake Bay region (Morse et al., 2014, Mulholland et al., 2018). Different species have different tolerances and physiological requirements, and these may not be well represented using the method of aggregate models. Finally, the mechanisms responsible for the termination of *M. polykrikoides* blooms are not fully understood, and the current model uses an artificial algorithm to make the bloom collapse at a time consistent with field observations. As shown in Fig. 2, the inability to simulate bloom termination accurately results in overestimates of algal cell density

during the late stages of blooms in some years. One possible mechanism whereby blooms terminate is through the loss of vegetative cells by the formation of resting cysts. Some studies have shown that after a bloom reaches a certain threshold, cyst-forming species may rapidly convert to sexual stages and undergo mass gametogenesis events (e.g., Brosnahan et al., 2017 and 2020). This could result in the production of resting cysts and may cause a complete termination of the bloom even if the environmental conditions still favor algal growth. Alternatively, storms and frontal systems have been implicated in the rapid termination of *M. polykrikoides* blooms (Filippino et al., 2017).

The current model does not simulate the complete life cycle of *M. polykrikoides*. The contribution of cyst germination and the subsequent release and loading of vegetative cells, $germ_{ini}$, into the water column is assumed to be completed within one day, and the release date in each year is based on the model calibration. The real "initial time" may deviate from the calibrated t_{ini} in the model, and the initial loading can also be different from the given $germ_{ini}$. Because of the large tidal excursion that mixes algae within a few tidal cycles, the calibration is to find a t_{ini} so that the modeled algal cell density with the given $germ_{ini}$ is close to the available observations within a few tidal cycles. In natural systems, it is more likely that cyst germination occurs over many days/weeks and the timing, varies among years due to differences in environmental factors such as bottom water temperature, oxygen, and cyst resuspension (e.g., Kremp and Anderson, 2000; Anderson et al., 2005; Anderson and Rengefors, 2006; McGill et al., in revision). We currently lack a comprehensive understanding of cyst germination in nature and this may require a comprehensive examination of environmental factors regulating germination. Although cyst distributions in sediments may regulate the initial spatial loading of vegetative cells, in the model the loading is the same over the entire area of the lower James and its

tributaries. Despite this, blooms still appeared to initiate in the Lafayette River because of how physical transport processes redistribute the released cells within a few tidal cycles in the study system with a relatively small area (Morse et al., 2013; Qin and Shen, 2019). The lack of information on cyst distributions, germination rates, and the interaction between water residence time and population development all hamper our ability to predict bloom initiation with certainty.

5. Conclusions

A numerical HAB module for *M. polykrikoides* bloom was developed, which includes three behavioral and life cycle strategies (mixotrophic growth, swimming behavior, and cyst germination). The HAB module was successfully incorporated into a 3D physical-biogeochemical numerical model. The model results show that behavioral and life cycle strategies contribute significantly to bloom development and dynamics in the lower James River and its tributaries (the Elizabeth and Lafayette Rivers). Both during the initiation period and in later stages, blooms are fueled by uptake of organic matter the heterotrophic growth rate is higher than the phototrophic growth rate. The resultant mixotrophic growth (phototrophic + heterotrophic) counterbalances the flushing and other unsuitable environmental conditions and ensures that *M. polykrikoides* can accumulate to bloom densities and achieve high growth rates. Swimming speed played a large role in *M. polykrikoides* bloom formation, altering the timing and magnitude of blooms. Model results also showed that the interannual variability in the timing of bloom initiation in the Lafayette River is regulated primarily by temperature, physical transport processes, and the process of cyst germination, while other environmental factors and behavioral strategies were less important.

Acknowledgements

The funding for this study is provided by Virginia Department of Environmental Quality through contracts 16633 to VIMS and 15425, 12582, and 15255 to ODU, by the Hampton Roads Sanitation District through contracts 14566 and 15696 to ODU, and by NOAA ECOHAB with grant number NA18NOS4780176 to ODU. We thank Todd Egerton for providing the data of *M. polykrikoides* cell abundance and critical reviews on the manuscript. We appreciate comments and suggestions from Mark Brush, Kyeong Park, Marjorie Friedrichs, and two anonymous reviewers. This paper is Contribution No. xxxx of the Virginia Institute of Marine Science, William & Mary.

Appendix. HAB module development

Gross growth rate

Margalefidinium polykrikoides is considered a constitutive mixotroph (Mitra et al., 2016), so its mixotrophic gross growth rate, G, can be contributed by both phototrophic growth and heterotrophic growth. In this module, the components of the gross growth rate from each growth mode (G^p for phototrophic and G^h for heterotrophic) are separately formulated and the mixotrophic gross growth rate is calculated based on the two components. Among limiting factors for *M. polykrikoides* growth, temperature, salinity, light irradiance, and nutrients were included in the model. The current model does not explicitly simulate allelopathy effects of *M. polykrikoides* on co-occurring algae, bacteria, and grazers (Tang and Gobler, 2010); or the effect of Vitamin B, a possible limiting factor under natural conditions as suggested in the literature (Tang et al., 2010; Koch et al., 2014).

Photoautotrophic growth

The gross growth rate for phototrophic growth is expressed as a function of temperature, salinity, light irradiance, and dissolved nutrient concentrations:

$$G_o^p = G_{opt}^p f(T) f(Sal) min[f(I), f(DIN), f(DIP)] \quad \text{(A1)}$$

Where G_o^p denotes G^p of *M. polykrikoides* if the growth is only through phototrophy, which can be different from the finalized G^p in the model. G_{opt}^p is the phototrophic gross growth rate at the optimal condition, $f(T)$, $f(Sal)$, $f(I)$, $f(DIN)$, $f(DIP)$ are the growth-limiting functions for temperature (T), salinity (Sal), irradiance (I), dissolved inorganic nitrogen (DIN), and dissolved inorganic phosphate (DIP), respectively, and their expressions are listed in Table 1. The photosynthesis-irradiance relationship for *M. polykrikoides* suggests that the half saturation

801 constant for light is about 30 μE m^{-2} s^{-1} and photoinhibition does not occur at photon fluxes of
802 less than 300 μE m^{-2} s^{-1} (Kim et al., 2004; Oh et al., 2006). The Monod type equation was
803 adopted for both nutrients and light limitations.

804 Heterotrophic growth

805 *Margalefidinium polykrikoides* can take up organic matter (OM) to maintain a high
806 heterotrophic growth rate (Jeong et al., 2004), and the sources include DOM, a fraction of POM
807 and organisms with size smaller than 12 μm, such as cryptophyte (Jeong et al., 2004) and
808 bacteria (Seong et al., 2006). Some studies have shown that the heterotrophic growth can be
809 affected by environmental conditions such as temperature, salinity, and light (e.g., Skovgaard,
810 1996; Hansen and Nielsen, 1997; Berge et al., 2008; Jeong et al., 2018; Lim et al., 2019; Ok et
811 al., 2019; You et al., 2020). Here, the heterotrophy is assumed to be a function of temperature
812 and salinity, as these two factors may regulate the activity of enzymes required for processes
813 involving heterotrophic growth. In this current model, because it is still unclear how light
814 influences the heterotrophic growth of *M. polykrikoides,* we did not consider the possible effect
815 of light and assumed heterotrophy can also occur in the dark. Nevertheless, the induced
816 uncertainty is minimalized by using an optimal heterotrophic growth rate G^h_{opt} lower than G^p_{opt} to
817 make the daily-averaged value of G^h_{opt} equal the measured value in the laboratory (Table 2).

818 Thus, the formulation for G^h is

819 $$G^h_o = G^h_{opt} f(T) f(Sal) f(OM_{12}), \quad \text{(A2)}$$

820 where G^h_o denotes G^h of *M. polykrikoides* if the growth is only through heterotrophy, which can
821 be different from the finalized G^h in the model. G^h_{opt} is the heterotrophic gross growth rate at the
822 optimal condition, $f(T)$ and $f(Sal)$ are assumed to be the same for phototrophic gross growth

rate G_o^p in Eq. (A1), and the Monod type equation was adapted for $f(OM_{12})$ following the culture experiment in Jeong et al. (2004). *M. polykrikoides* can engulf particulate organic matter (POM) via phagotrophy and take up dissolved organic matter (DOM) via osmotrophy. In the numerical model, a fraction (< 12 μm) of the other two groups of algae besides *M. polykrikoides* and other POM contributes to the phagotrophic growth, while DOM contributes to the osmotrophic growth. Thus, the available organic matter, OM_{12}, is provided by the two groups of simulated algae, $\sum_i b_i C_i$, and also by the other organic matter (including both particulate and dissolved), OM_{dead}; $OM_{12} = \sum_i b_i C_i + OM_{dead}$, where b is the fraction of organisms smaller than 12 μm, with i = 2 or 3 indicating the index of algae group, and

$$OM_{dead} = min\begin{Bmatrix} DOC + a_{1C}RPOC + a_{2C}LPOC, \\ (DON + a_{1N}RPON + a_{2N}LPON)/ANC, \\ (DOP + a_{1P}RPOP + a_{2P}LPOP)/APC \end{Bmatrix},$$

where ANC and APC are nitrogen to carbon ratio and phosphate to carbon ratio, respectively. Correspondingly, the uptake of organic matter corresponding to mixotrophic growth is $G^h C$, and it contributes to kinetic equations for the other two simulated phytoplankton species, dissolved organic carbon (DOC), refractory particulate organic carbon (RPOC), labile particulate organic carbon (LPOC), dissolved organic nitrogen (DON), refractory particulate organic nitrogen (RPON), labile particulate organic nitrogen (LPON), dissolved organic phosphate (DOP), refractory particulate organic phosphate (RPOP), and labile particulate organic phosphate (LPOP), while coefficient *a* denotes the fraction of POM besides prey algae that is smaller than 12 μm, and a_{1C}, a_{2C}, a_{1N}, a_{2N}, a_{1P}, and a_{2P} are the fraction for each component, respectively. Note that this model does not simulate bacteria explicitly, and bacteria is implicitly included in POM besides prey algae.

In the model, the contribution (recycle) to the nutrient pool is calculated by adding a sink term ($-G^h C\chi$) for each kinetic equation, where χ denotes the fractions of each component resembling OM_{12}, respectively. Specifically, the corresponding sink term for the dynamics of the other two phytoplankton species is expressed as:

$$Phytoplankton\ i\colon \chi_i = \frac{b_i C_i}{OM_{12}}, i = 2\ or\ 3$$

For carbon cycle:

$$DOC\colon \chi_{1C} = \frac{OM_{dead}}{OM_{12}} \frac{DOC}{DOC + a_{1C}RPOC + a_{2C}LPOC}$$

$$RPOC\colon \chi_{2C} = \frac{OM_{dead}}{OM_{12}} \frac{a_{1C}RPOC}{DOC + a_{1C}RPOC + a_{2C}LPOC}$$

$$LPOC\colon \chi_{3C} = \frac{OM_{dead}}{OM_{12}} \frac{a_{2C}LPOC}{DOC + a_{1C}RPOC + a_{2C}LPOC}$$

nitrogen cycle:

$$DON\colon \chi_{1N} = \frac{OM_{dead}}{OM_{12}} \frac{DON}{DON + a_{1N}RPON + a_{2N}LPON} ANC$$

$$RPON\colon \chi_{2N} = \frac{OM_{dead}}{OM_{12}} \frac{a_{1N}RPON}{DON + a_{1N}RPON + a_{2N}LPON} ANC$$

$$LPON\colon \chi_{3N} = \frac{OM_{dead}}{OM_{12}} \frac{a_{2N}LPON}{DON + a_{1N}RPON + a_{2N}LPON} ANC$$

and phosphate cycle:

$$DOP\colon \chi_{1P} = \frac{OM_{dead}}{OM_{12}} \frac{DOP}{DOP + a_{1P}RPOP + a_{2P}LPOP} APC$$

$$RPOP: \chi_{2P} = \frac{OM_{dead}}{OM_{12}} \frac{a_{1P} RPOP}{DOP + a_{1P} RPOP + a_{2P} LPOP} APC$$

$$LPOP: \chi_{3P} = \frac{OM_{dead}}{OM_{12}} \frac{a_{2P} LPOP}{DOP + a_{1P} RPOP + a_{2P} LPOP} APC$$

Mixotrophic growth (photoautotrophic + heterotrophic growths)

Without considering interactions between phototrophic growth and heterotrophic growth, the gross growth rate for mixotrophic growth can be expressed as a combination of phototrophic growth and heterotrophic growth $\left(G_o^p + G_o^h\right)$. It is apparent that the mixotrophic rate, G, equals the heterotrophic rate, G_o^h, during the nighttime. During the daytime, however, G cannot exceed the maximum growth rate that *M. polykrikoides* can reach under the given environmental condition (Ghyoot et al., 2017a), which at a certain temperature and salinity is $G_{opt}^p f(T) f(Sal)$. Thus, G has the formula:

$$\begin{aligned} G &= min\left[G_o^p + G_o^h, G_{opt}^p f(T) f(Sal)\right] \quad (Daytime) \\ G &= G_o^h \qquad\qquad\qquad\qquad\qquad\quad (Nighttime) \end{aligned} \tag{A3}$$

During the nighttime, only heterotrophic growth exists, and the finalized G^h resulted in the model equals G_o^h. During the daytime, two options of computing the finalized G^p and the finalized G^h are included in the module for the case $\left(G_o^p + G_o^h\right) > G_{opt}^p f(T) f(Sal)$, based on the preference of which growth mode this algal species uses primarily. If phototrophy is favored and the heterotrophy only complements the total growth, the finalized G^p and the finalized G^h equal:

$$\begin{aligned} G^p &= G_o^p \qquad\qquad\qquad\qquad\quad (Daytime) \\ G^h &= \left[G_{opt}^p f(T) f(Sal) - G_o^p\right] \quad (Daytime) \\ G^h &= G_o^h \qquad\qquad\qquad\qquad\quad (Nighttime) \end{aligned} \tag{A4}$$

If there is no preference of using the growth modes, then the finalized G^p and the finalized G^h are calculated, respectively:

$$\begin{aligned} G^p &= G^p_{opt} f(T) f(Sal) \cdot G^p_o / \left(G^p_o + G^h_o\right) \quad (Daytime) \\ G^h &= G^p_{opt} f(T) f(Sal) \cdot G^h_o / \left(G^p_o + G^h_o\right) \quad (Daytime) \\ G^h &= G^h_o \quad (Nighttime) \end{aligned} \tag{A5}$$

Currently in the module, favoring phototrophy is defaulted for *M. polykrikoides* growth.

In addition, for the convenience, the mixotrophic growth rate, G, at any time is simply notated in the study as:

$$G = G_{opt} f(T) f(Sal) f(Res) \tag{A6}$$

where $f(Res)$ denotes the total contribution of resource species (light, inorganic nutrients, and bioavailable organic matter) to G. Clearly, G_{opt} equals G^p_{opt} during the daytime and G^h_{opt} during the nighttime. The notation $G_{TS} = G_{opt}\, f(T) f(Sal)$ was also used, which describes the potential highest gross growth rate limited by temperature and salinity (i.e., resources are not limited).

Carbon to chl-a ratio

For *M. polykrikoides*, Noh et al. (2018) reported that the chl-a content of the cultured strain is 30 pg chl-a cell^{-1}, i.e., 30 μg chl-a l^{-1} per 1000 cells ml^{-1}. In the numerical model, a constant carbon to chl-a ratio (C:Chl) was used. The chl-a content is assumed to be 30 pg chl-a cell^{-1} that was obtained from a laboratory measurement (Noh et al., 2018), and the corresponding C:Chl is 60.6 g C / g chl-a.

Loss terms

The sink of *M. polykrikoides* biomass may include the respiration/excretion, grazing, degradation by bacteria (e.g., Park et al., 2015), and resting cysts germination.

In the model, the basic metabolism (respiration/excretion) is a function of temperature. The respiratory loss due to photosynthesis is an additional metabolism to respiration/excretion, and the ratio to phototrophic growth rate, f^p, is estimated from the curve between specific growth rate and light irradiance. The degradation by bacteria is not explicitly considered, which is implicitly included in the metabolism in the model. The loss to grazers is assumed to be suppressed for simplicity. According to literature, the harmful effects of *M. polykrikoides* to organisms become significant when their density reaches a threshold level, e.g., 330 cells ml^{-1} (Tang and Gobler, 2009; Gobler et al., 2012). Thus, a mortality rate, *M*, was assumed to equal zero in the model for the James River.

The resting cysts are generally produced in the intense phase of a HAB event, but the mechanisms of forming resting cysts are still not clear (Brosnahan et al., 2020). Some studies suggest that the resting cyst formation occurs when the environmental conditions are not suitable, such as scarcity of macronutrients. Other studies suggest that the formation of resting cysts is endogenous or 'clock'-regulated (e.g., Anderson and Keafer, 1987). In the model, the loss due to the formation of resting cysts is not included.

For the termination of *M. polykrikoides* blooms, observations show that the bloom usually declines after September of the year and eventually disappears. Data analysis shows that within one year, the temperature is suitable for *M. polykrikoides* growth from May to June in this region, and it can be a significant limiting factor during the high-temperature period (e.g., August). However, it becomes suitable again from late September through October. If vegetative

cells of *M. polykrikoides* could survive to the second suitable period for temperature, they could grow again with a high growth rate and cause a bloom. This suggests that there must be some unknown mechanisms causing the decline of *M. polykrikoides* blooms and prevent their return. While a mandatory dormancy for resting cysts may prevent the re-initiation of the bloom (Kremp and Anderson, 2000), the mechanisms for the collapse still remain unknown, and hypotheses may include the unsuitable environmental conditions (e.g., shortage of nutrients), resting cyst formation, parasitism, and aggregation. In numerical modeling, the collapse is implicitly considered. To be consistent with observations, the gross growth rate is assumed to be zero after mid-September every year, and *M. polykrikoides* cells are entirely removed from the water column by September 26.

Swimming

The swimming ability of dinoflagellates allows the cells to change their vertical position in the water column, and studies suggest that in the daytime, *M. polykrikoides* can swim up to the near surface where the potential to receive high light irradiance is better (Kudela and Gobler, 2012). The maximum swimming speed of *M. polykrikoides* is reported to be 1449 $\mu m\ s^{-1}$ (Jeong et al., 2015). The swimming behavior is modeled with the measured values of speed in Sohn et al. (2011), where they observed in laboratory that the mean swimming speeds at 22 °C for single cell, two-, four-, and eight-cell chain are 391, 599, 800, 856 $\mu m\ s^{-1}$, respectively. Chain-formation provides them a more competitive advantage in receiving light (Kudela and Gobler, 2012). The corresponding velocities are 34–74 m d^{-1}, respectively. In the module, the swimming speed is set to be w_c = 55 m d^{-1}, and the cells are only allowed to swim upward. In addition, it is possible that the upward swimming can stop at those layers where the light irradiance is not a limiting factor. At night there may not be a specific swimming direction for swimming, and

929 therefore the vertical swimming speed is set to be zero in the model. The vertical mixing,
930 nevertheless, can transport surface cells to the lower layers.

931 *Cyst germination*

932 The external source of vegetative *M. polykrikoides* is from the germination of resting
933 cysts (input from the germination of temporary cyst is omitted). In reality, the loading rate of
934 vegetative cells by cyst germination depends on the cyst density in sediment and the germination
935 process that are influenced by environmental conditions such as temperature.

936 In this model, this process is incorporated implicitly by assuming an initial loading of
937 vegetative cells ($germ_{ini}$ = 25000 cells m^{-2} d^{-1} in this study) into the bottom layer for one day on a
938 chosen date of the year. This assumption avoids the uncertainties in the temporal variability in
939 the germination rate.

References

Aleynik, D., Dale, A.C., Porter, M. and Davidson, K., 2016. A high resolution hydrodynamic model system suitable for novel harmful algal bloom modelling in areas of complex coastline and topography. Harmful algae, 53, 102-117.

Anderson, C.R., Moore, S.K., Tomlinson, M.C., Silke, J. and Cusack, C.K., 2015. Living with harmful algal blooms in a changing world: strategies for modeling and mitigating their effects in coastal marine ecosystems. In *Coastal and Marine Hazards, Risks, and Disasters* (pp. 495-561). Elsevier.

Anderson, D.M., Glibert, P.M., Burkholder, J.M., 2002. Harmful algal blooms and eutrophication: nutrient sources, composition, and consequences. Estuaries, 25(4), 704-726.

Anderson, D.M., Rengefors, K., 2006. Community assembly and seasonal succession of marine dinoflagellates in a temperate estuary: the importance of life cycle events. Limnol. Oceanogr. 51(2), 860-873.

Anderson, D.M., Keafer, B.A., 1987. An endogenous annual clock in the toxic marine dinoflagellate *Gonyaulax tamarensis*. Nature 325(6105), 616.

Anderson, D.M., Stock, C.A., Keafer, B.A., Nelson, A.B., Thompson, B., McGillicuddy Jr, D.J., Keller, M., Matrai, P.A. and Martin, J., 2005. *Alexandrium fundyense* cyst dynamics in the Gulf of Maine. Deep Sea Res. Part II Top. Stud. Oceanogr. 52(19-21), 2522-2542.

959 Anderson, D.M., Stolzenbach, K.D., 1985. Selective retention of two dinoflagellates in a well-
960 mixed estuarine embayment: the importance of diel vertical migration and surface
961 avoidance. Mar. Ecol. Prog. Ser., 39-50.

962 Azanza, R.V., Brosnahan, M.L., Anderson, D.M., Hense, I., Montresor, M., 2018. The role of
963 life cycle characteristics in harmful algal bloom dynamics. In: Glibert, P., Berdalet, E.,
964 Burford, M., Pitcher, G., Zhou, M. (Eds.), Global Ecology and Oceanography of Harmful
965 Algal Blooms. Ecological Studies (Analysis and Synthesis). Springer.

966 Berge, T., Hansen, P.J. and Moestrup, Ø., 2008. Feeding mechanism, prey specificity and growth
967 in light and dark of the plastidic dinoflagellate *Karlodinium armiger*. Aquat. Microb.
968 Ecol. 50(3), 279-288.

969 Brosnahan, M.L., Ralston, D.K., Fischer, A.D., Solow, A.R. and Anderson, D.M., 2017. Bloom
970 termination of the toxic dinoflagellate *Alexandrium catenella*: Vertical migration
971 behavior, sediment infiltration, and benthic cyst yield. Limnol. Oceanogr. 62(6), 2829-
972 2849.

973 Burkholder, J.M., Glibert, P.M., Skelton, H., 2008. Mixotrophy, a major mode of nutrition for
974 harmful algal species in eutrophic waters. Harmful Algae 8, 77–93.

975 Cloern, J.E., Grenz, C., Vidergar-Lucas, L., 1995. An empirical model of the phytoplankton
976 chlorophyll: carbon ratio-the conversion factor between productivity and growth
977 rate. Limnol. Oceanogr. 40(7), 1313-1321.

978 Filippino, K.C., Egerton, T.A., Hunley, W.S., Mulholland, M.R., 2017. The influence of storms
979 on water quality and phytoplankton dynamics in the tidal James River. Estuaries and
980 Coasts, 40(1), 80-94.

Flynn, K.J., McGillicuddy, J.D.J., 2018. Modeling marine harmful algal blooms; Current status and future prospects. In: SE, S, J-AM, B, S., M (Eds.), Harmful Algal Blooms: A Compendium Desk Reference. Wiley Science Publishers.

Flynn, K.J., Mitra, A., 2009. Building the "perfect beast": modelling mixotrophic plankton. J. Plankton Res. 31(9), 965-992.

Flynn, K.J., Mitra, A., Glibert, P.M., Burkholder, J.-A.M., et al., 2018. Mixotrophy in harmful algal blooms: by whom, on whom, when, why, and what next. In: Glibert, P.M. (Ed.), Ecological Studies 232, Global Ecology and Oceanography of Harmful Algal Blooms. Springer.

Franks, P.J., 2018. Recent advances in modelling of harmful algal blooms. In *Global Ecology and Oceanography of Harmful Algal Blooms* (pp. 359-377). Springer, Cham.

Garcés, E., Bravo, I., Vila, M., Figueroa, R.I., Masó, M. and Sampedro, N., 2004. Relationship between vegetative cells and cyst production during Alexandrium minutum bloom in Arenys de Mar harbour (NW Mediterranean). J. Plankton Res. 26(6), 637-645.

Gentien, P., Lunven, M., Lazure, P., Youenou, A. and Crassous, M.P., 2007. Motility and autotoxicity in *Karenia mikimotoi* (Dinophyceae). Philos. Trans. R. Soc., B 362(1487), 1937-1946.

Ghyoot, C., Flynn, K.J., Mitra, A., Lancelot, C., Gypens, N., 2017a. Modeling Plankton Mixotrophy: A Mechanistic Model Consistent with the Shuter-Type Biochemical Approach. Front. Ecol. Evol. 5, p.78.

1001 Ghyoot, C., Lancelot, C., Flynn, K.J., Mitra, A. and Gypens, N., 2017b. Introducing mixotrophy
1002 into a biogeochemical model describing an eutrophied coastal ecosystem: The Southern
1003 North Sea. Prog. Oceanogr. 157, 1-11.

1004 Gillibrand, P.A., Siemering, B., Miller, P.I. and Davidson, K., 2016. Individual-based modelling
1005 of the development and transport of a *Karenia mikimotoi* bloom on the North-west
1006 European continental shelf. Harmful algae 53, 118-134.

1007 Glibert, P.M., Allen, J.I., Bouwman, A.F., Brown, C.W., Flynn, K.J., Lewitus, A.J. and Madden,
1008 C.J., 2010. Modeling of HABs and eutrophication: status, advances, challenges. J. Marine
1009 Syst. 83(3-4), 262-275.

1010 Gobler, C.J., Burson, A., Koch, F., Tang, Y., Mulholland, M.R., 2012. The role of nitrogenous
1011 nutrients in the occurrence of harmful algal blooms caused by *Cochlodinium*
1012 *polykrikoides* in New York estuaries (USA). Harmful Algae 17, 64-74.

1013 Gómez, F., Richlen, M.L., Anderson, D.M., 2017. Molecular characterization and morphology of
1014 *Cochlodinium strangulatum*, the type species of *Cochlodinium*, and *Margalefidinium* gen.
1015 nov. for *M. polykrikoides* and allied species (Gymnodiniales, Dinophyceae). Harmful
1016 Algae 63, 32-44.

1017 Hansen P.J., Nielsen T.G., 1997. Mixotrophic feeding of *Fragilidium subglobosum*
1018 (Dinophyceae) on three species of *Ceratium*: effects of prey concentration, prey species
1019 and light intensity. Mar. Ecol. Prog. Ser. 147,187-196.

1020 Heisler, J., Glibert, P.M., Burkholder, J.M., Anderson, D.M., Cochlan, W., Dennison, W.C.,
1021 Dortch, Q., Gobler, C.J., Heil, C.A., Humphries, E., Lewitus, A., 2008. Eutrophication
1022 and harmful algal blooms: a scientific consensus. Harmful Algae 8(1), 3-13.

1023 Hong, B., Shen, J., Xu, H., 2018. Upriver transport of dissolved substances in an estuary and
1024 sub-estuary system of the lower James River, Chesapeake Bay. Front. Earth Sci. 1-17.

1025 Jeong, H.J., Lee, K.H., Du Yoo, Y., Kang, N.S., Song, J.Y., Kim, T.H., Seong, K.A., Kim, J.S.
1026 and Potvin, E., 2018. Effects of light intensity, temperature, and salinity on the growth
1027 and ingestion rates of the red-tide mixotrophic dinoflagellate *Paragymnodinium*
1028 *shiwhaense*. Harmful algae 80, 46-54.

1029 Jeong, H.J., Lim, A.S., Franks, P.J., Lee, K.H., Kim, J.H., Kang, N.S., Lee, M.J., Jang, S.H., Lee,
1030 S.Y., Yoon, E.Y., Park, J.Y., 2015. A hierarchy of conceptual models of red-tide
1031 generation: nutrition, behavior, and biological interactions. Harmful Algae 47, 97-115.

1032 Jeong, H.J., Yoo, Y.D., Kim, J.S., Kim, T.H., Kim, J.H., Kang, N.S., Yih, W., 2004. Mixotrophy
1033 in the phototrophic harmful alga *Cochlodinium polykrikoides* (Dinophycean): prey
1034 species, the effects of prey concentration, and grazing impact. J. Eukaryotic
1035 Microbiol. 51(5), 563-569.

1036 Jiang, X., Tang, Y., Lonsdale, D.J., Gobler, C.J., 2009. Deleterious consequences of a red tide
1037 dinoflagellate *Cochlodinium polykrikoides* for the calanoid copepod *Acartia tonsa*. Mar.
1038 Ecol. Prog. Ser. 390, 105–116.

1039 Jones, H., 1997. A classification of mixotrophic protists based on their behaviour. *Freshwater*
1040 *Biology*, *37*(1), 35-43.

1041 Kim, D.I., Matsuyama, Y., Nagasoe, S., Yamaguchi, M., Yoon, Y.H., Oshima, Y., Imada, N.,
1042 Honjo, T., 2004. Effects of temperature, salinity and irradiance on the growth of the
1043 harmful red tide dinoflagellate *Cochlodinium polykrikoides* Margalef (Dinophyceae). J.
1044 Plankton Res. 26(1), 61-66.

1045 Kim, H.C., Lee, C.K., Lee, S.G., Kim, H.G., Park, C.K., 2001. Physico-chemical factors on the
1046 growth of *Cochlodinium polykrikoides* and nutrient utilization. Korean J. Fish. Aquat.
1047 Sci. 34(5), 445-456.

1048 Koch, F., Burson, A., Tang, Y.Z., Collier, J.L., Fisher, N.S., Sanudo-Wilhelmy, S., Gobler, C.J.,
1049 2014. Alteration of plankton communities and biogeochemical cycles by harmful
1050 *Cochlodinium polykrikoides* (Dinophyceae) blooms. Harmful Algae 33, 41-54.

1051 Kremp, A., Anderson, D.M., 2000. Factors regulating germination of resting cysts of the spring
1052 bloom dinoflagellate *Scrippsiella hangoei* from the northern Baltic Sea. J. Plankton Res.
1053 22(7), 1311-1327.

1054 Kudela, R., Gobler, C.J., 2012. Harmful dinoflagellate blooms caused by *Cochlodinium* sp.:
1055 global expansion and ecological strategies facilitating bloom formation. Harmful Algae
1056 14, 71–86.

1057 Kudela, R.M., Ryan, J.P., Blakely, M.D., Lane, J.Q., Peterson, T.D., 2008. Linking the
1058 physiology and ecology of *Cochlodinium* to better understand harmful algal bloom events:
1059 a comparative approach. Harmful Algae 7(3), 278-292.

1060 Lim, A.S., Jeong, H.J., Jang, T.Y., Jang, S.H. and Franks, P.J., 2014. Inhibition of growth rate
1061 and swimming speed of the harmful dinoflagellate *Cochlodinium polykrikoides* by
1062 diatoms: implications for red tide formation. Harmful Algae, 37, 53-61.

1063 Lim, A.S., Jeong, H.J., Ok, J.H., You, J.H., Kang, H.C. and Kim, S.J., 2019. Effects of light
1064 intensity and temperature on growth and ingestion rates of the mixotrophic dinoflagellate
1065 *Alexandrium pohangense*. Mar. Biol. 166, 98.

Lin, C.H., Flynn, K.J., Mitra, A., Glibert, P.M., 2018. Simulating effects of variable stoichiometry and temperature on mixotrophy in the harmful dinoflagellate *Karlodinium veneficum*. Front. Mar. Sci. 5: 320.

Marshall, H.G., 2009. Phytoplankton of the York river. J. Coast. Res. 57, 59-65.

McGillicuddy Jr, D.J., 2010. Models of harmful algal blooms: conceptual, empirical, and numerical approaches. J. Marine Syst. 83(3-4), 105-107.

McGillicuddy Jr, D.J., Anderson, D.M., Lynch, D.R. and Townsend, D.W., 2005. Mechanisms regulating large-scale seasonal fluctuations in *Alexandrium fundyense* populations in the Gulf of Maine: results from a physical–biological model. Deep Sea Res., Part II 52(19-21), 2698-2714.

Milroy, S.P., Dieterle, D.A., He, R., Kirkpatrick, G.J., Lester, K.M., Steidinger, K.A., Vargo, G.A., Walsh, J.J. and Weisberg, R.H., 2008. A three-dimensional biophysical model of *Karenia brevis* dynamics on the west Florida shelf: A look at physical transport and potential zooplankton grazing controls. Cont. Shelf Res. 28(1):112-136.

Mitra, A., Flynn, K.J., Tillmann, U., Raven, J.A., Caron, D., Stoecker, D.K., Not, F., Hansen, P.J., Hallegraeff, G., Sanders, R. and Wilken, S., 2016. Defining planktonic protist functional groups on mechanisms for energy and nutrient acquisition: incorporation of diverse mixotrophic strategies. Protist 167(2), 106-120.

Moore, S.K., Johnstone, J.A., Banas, N.S. and Salathe Jr, E.P., 2015. Present-day and future climate pathways affecting *Alexandrium* blooms in Puget Sound, WA, USA. Harmful Algae 48, 1-11.

Morse, R. E., Mulholland, M. R., Hunley, W. S., Fentress, S., Wiggins, M., Blanco-Garcia, J. L., 2013. Controls on the initiation and development of blooms of the dinoflagellate *Cochlodinium polykrikoides* Margalef in lower Chesapeake Bay and its tributaries. Harmful Algae 28, 71-82.

Morse, R.E., Mulholland, M.R., Egerton, T.A. and Marshall, H.G., 2014. Phytoplankton and nutrient dynamics in a tidally dominated eutrophic estuary: daily variability and controls on bloom formation. Mar. Ecol. Prog. Ser. 503, 59-74.

Morse, R.E., Shen, J., Blanco-Garcia, J.L., Hunley, W.S., Fentress, S., Wiggins, M., Mulholland, M.R., 2011. Environmental and physical controls on the formation and transport of blooms of the dinoflagellate *Cochlodinium polykrikoides* Margalef in the lower Chesapeake Bay and its tributaries. Estuaries Coasts 34(5), 1006-1025.

Mulholland, M.R., Morse, R., Egerton, T., Bernhardt, P.W., Filippino, K.C., 2018. Blooms of Dinoflagellate Mixotrophs in a Lower Chesapeake Bay Tributary: Carbon and Nitrogen Uptake over Diurnal, Seasonal, and Interannual Timescales. Estuaries Coasts 41(6), 1-22.

Mulholland, M.R., Morse, R.E., Boneillo, G.E., Bernhardt, P.W., Filippino, K.C., Procise, L.A., Blanco-Garcia, J.L., Marshall, H.G., Egerton, T.A., Hunley, W.S., Moore, K.A., Berry, D.L., Gobler, C.J., 2009. Understanding causes and impacts of the dinoflagellate, *Cochlodinium polykrikoides*, blooms in the Chesapeake Bay. Estuaries Coasts 32, 734–747.

Noh, J.H., Kim, W., Son, S.H., Ahn, J.H., Park, Y.J., 2018. Remote quantification of *Cochlodinium polykrikoides* blooms occurring in the East Sea using geostationary ocean color imager (GOCI). Harmful Algae 73, 129-137.

Oh, S.J., Yoon, Y.H., Kim, D.I., Shimasaki, Y., Oshima, Y., Honjo, T., 2006. Effects of Light Quantity and Quality on the Growth of the Harmful Dinoflagellate, *Cochlodinium polykrikoides* Margalef (Dinophyceae). Algae 21(3), 311-316.

Park, B.S., Kim, J.H., Kim, J.H., Gobler, C.J., Baek, S.H., Han, M.S., 2015. Dynamics of bacterial community structure during blooms of *Cochlodinium polykrikoides* (Gymnodiniales, Dinophyceae) in Korean coastal waters. Harmful Algae 48, 44-54.

Phlips, E.J., Badylak, S., Nelson, N.G., Havens, K.E., 2020. Hurricanes, El Niño and harmful algal blooms in two sub-tropical Florida estuaries: Direct and indirect impacts. Scientific reports, 10(1), 1-12.

Qin, Q., Shen, J., 2017. The contribution of local and transport processes to phytoplankton biomass variability over different timescales in the Upper James River, Virginia. Estuar. Coast. Shelf Sci. 196, 123-133.

Qin, Q., Shen, J., 2019. Physical transport processes affect the origins of harmful algal blooms in estuaries. Harmful algae 84, 210-221.

Qin, Q., Shen, J., 2021. Applying transport rate for quantifying local transport conditions in estuarine and coastal systems. J. Mar. Syst. 218, p.103542.

Ralston, D.K., Brosnahan, M.L., Fox, S.E., Lee, K.D., Anderson, D.M., 2015. Temperature and residence time controls on an estuarine harmful algal bloom: Modeling hydrodynamics and *Alexandrium fundyense* in Nauset Estuary. Estuaries Coasts 38(6), 2240-2258.

Ralston, D.K., Keafer, B.A., Brosnahan, M.L., Anderson, D.M., 2014. Temperature dependence of an estuarine harmful algal bloom: Resolving interannual variability in bloom dynamics using a degree-day approach. Limnol. Oceanogr. 59(4), 1112-1126.

Ralston, D.K., Moore, S.K., 2020. Modeling harmful algal blooms in a changing climate. Harmful Algae, 91, 101729. doi.org/10.1016/j.hal.2019.101729

Scully, M.E., 2010. The importance of climate variability to wind-driven modulation of hypoxia in Chesapeake Bay. J. Phys. Oceanogr. 40(6), 1435-1440.

Scully, M.E., 2010. Wind modulation of dissolved oxygen in Chesapeake Bay. Estuaries Coasts 33(5), 1164-1175.

Scully, M.E., Friedrichs, C., Brubaker, J., 2005. Control of estuarine stratification and mixing by wind-induced straining of the estuarine density field. Estuaries 28(3), 321-326.

Seong, K.A., Jeong, H.J., Kim, S., Kim, G.H., Kang, J.H., 2006. Bacterivory by co-occurring red-tide algae, heterotrophic nanoflagellates, and ciliates. Mar. Ecol. Prog. Ser. 322, 85-97.

Shen, J., and Qin, Q., 2019. James River Water Quality Model Refinement and Scenario Simulations. Special Reports in Applied Marine Science and Ocean Engineering (SRAMSOE) No. 474. Virginia Institute of Marine Science, William & Mary. doi: 10.25773/j0fa-yk48

Shen, J., Wang, Y., Sisson, M., 2016. Development of the Hydrodynamic Model for Long-Term Simulation of Water Quality Processes of the Tidal James River, Virginia. J. Mar. Sci. Eng. 4(4), 82.

1149 Shin, H.H., Li, Z., Yoon, Y.H., Oh, S.J., Lim, W.A., 2017. Formation and germination of
1150 temporary cysts of *Cochlodinium polykrikoides* Margalef (Dinophyceae) and their
1151 ecological role in dense blooms. Harmful Algae 66, 57-64.

1152 Skovgaard A., 1996. Mixotrophy in Fragilidium subglobosum (Dinophyceae): growth and
1153 grazing responses as functions of light intensity. Mar. Ecol. Prog. Ser. 143, 247–253.

1154 Smayda, T.J., 2002. Turbulence, watermass stratification and harmful algal blooms: an
1155 alternative view and frontal zones as "pelagic seed banks". Harmful Algae 1(1), 95-112.

1156 Sohn, M.H., Seo, K.W., Choi, Y.S., Lee, S.J., Kang, Y.S., Kang, Y.S., 2011. Determination of
1157 the swimming trajectory and speed of chain-forming dinoflagellate Cochlodinium
1158 polykrikoides with digital holographic particle tracking velocimetry. Marine
1159 biology 158(3), 561-570.

1160 Stoecker, D.K., 1998. Conceptual models of mixotrophy in planktonic protists and some
1161 ecological and evolutionary implications. *Eur. J. Protistol. 34*(3), 281-290.

1162 Stoecker, D.K., Hansen, P.J., Caron, D.A. and Mitra, A., 2017. Mixotrophy in the marine
1163 plankton. Annu. Rev. Mar. Sci. 9, 311-335.

1164 Tang, Y.Z., Gobler, C.J., 2010. Allelopathic effects of *Cochlodinium polykrikoides* isolates and
1165 blooms from the estuaries of Long Island, New York, on co-occurring phytoplankton.
1166 Mar. Ecol. Prog. Ser. 406, 19-31.

1167 Tang, Y.Z., Gobler, C.J., 2012. The toxic dinoflagellate *Cochlodinium polykrikoides*
1168 (Dinophyceae) produces resting cysts. Harmful Algae 20, 71-80.

Tang, Y.Z., Koch, F., Gobler, C.J., 2010. Most harmful algal bloom species are vitamin B1 and B12 auxotrophs. Proc. Natl. Acad. Sci. U.S.A. 107(48), 20756-20761.

Virginia DEQ, 2019. Recommended Numeric Chlorophyll-a Criteria for the James River Estuary.

Wang, D.P., Elliott, A.J., 1978. Non-tidal variability in the Chesapeake Bay and Potomac River: Evidence for non-local forcing. J. Phys. Oceanogr. 8(2), 225-232.

Wells, W.L., Karlson, B., Wulff, A., Kudela, R.M., Trick, C., Asnaghi, V., Berdalet, E., Cochlan, W., Davidson, K., DeRijcke, M., Dutkiewicz, S., Hallegraeff, G., Flynn, K.J., Legrand, C., Paerl, H.W., Silke, J., Suikkanen, S., Thompson, P., Trainer, V.L., 2020. Future HAB science: directions and challenges in a changing climate. Harmful Algae 91, 101632. https://doi.org/10.1016/j.hal.2019.101632.

You, J.H., Jeong, H.J., Lim, A.S., Ok, J.H. and Kang, H.C., 2020. Effects of irradiance and temperature on the growth and feeding of the obligate mixotrophic dinoflagellate *Gymnodinium smaydae*. Mar. Biol. 167, 1-13.

Zhang, F., Li, M., Glibert, P.M. and Ahn, S.H.S., 2021. A three-dimensional mechanistic model of *Prorocentrum minimum* blooms in eutrophic Chesapeake Bay. Sci. Total Environ., 769, p.144528.

1186 Table 1. The *M. polykrikoides* model structure.

Abbreviation	Description	Expression
G^p	Phototrophic gross growth rate	See Eqs. A1, A4, and A5
G^h	Heterotrophic gross growth rate	See Eq. A2, A4, and A5
G	(Mixotrophic) gross growth rate	$G = G^p + G^h$; see Eqs. A3 and A6
$f(T)$	Growth-limiting function for temperature	$f(T) = e^{-k_{T1}\left(T-T_{opt}\right)^2}, T \le T_{opt}$ $f(T) = e^{-k_{T2}\left(T-T_{opt}\right)^2}, T > T_{opt}$
$f(Sal)$	Growth-limiting function for salinity	$f(Sal) = e^{-k_{Sal1}\left(Sal-Sal_{opt}\right)^2}, Sal \le Sal_{opt}$ $f(Sal) = e^{-k_{Sal2}\left(Sal-Sal_{opt}\right)^2}, Sal > Sal_{opt}$
$f(DIN)$	Growth-limiting function for DIN	$f(DIN) = \frac{DIN}{DIN+N_k}$
$f(DIP)$	Growth-limiting function for DIP	$f(DIP) = \frac{DIP}{DIP+P_k}$
$f(I)$	Growth-limiting function for light irradiance	$f(I) = \frac{I}{I+I_k}$
$f(OM_{12})$	Growth-limiting function for organic matter smaller than 12 μm	$f(OM_{12}) = \frac{OM_{12}}{OM_{12}+OM_{12k}}$
R	Respiration/excretion rate	$R = R_0\theta_R^{T-20} + f^p G^p$

1187

1188

Table 2. The *M. polykrikoides* model parameters and the values used in the experimental treatments. Most values were estimated based on the reported results from published laboratory experiments, the others are calibrated numerically. The optimal condition means the growth is not limiting by any environmental factor at all.

Abbr.	Description	Unit	Value	Reference
G_{opt}^{p}	Phototrophic gross growth rate at the optimal condition	d^{-1}	1.06	Gobler et al. (2012)
G_{opt}^{h}	Heterotrophic gross growth rate at the optimal condition	d^{-1}	0.62	Gobler et al. (2012)
f^{p}	respiratory losses associated with photosynthesis as a ratio to G^{p}		0.16	Gobler et al. (2012)
R_0	Basic metabolism rate at 20 °C	d^{-1}	0.025	Calibrated
w_c	Swimming velocity of *M. polykrikoides*	$m\ d^{-1}$	55	Sohn et al. (2011)
T_{opt}	Optimal temperature for growth	°C	25.1	Kim et al. (2004); Griffith and Gobler (2016)
k_{T1}	Temperature effect on growth below T_{opt}	$°C^{-2}$	0.0230	Kim et al. (2004); Griffith and Gobler (2016)
k_{T2}	Temperature effect on growth above T_{opt}	$°C^{-2}$	0.0277	Kim et al. (2004); Griffith and Gobler (2016)
Sal_{opt}	Optimal salinity for growth		34	Kim et al. (2004)
k_{Sal1}	Salinity effect on growth below Sal_{opt}		0.0024	Kim et al. (2004)
k_{Sal2}	Salinity effect on growth below Sal_{opt}		0.0222	Kim et al. (2004)
I_{opt}	Half-saturation coefficient for light irradiance	$\mu E\ m^{-2}\ s^{-1}$	30	Kim et al. (2004) and Oh et al. (2006)
N_k	Half-saturation coefficient for DIN	$g\ N\ m^{-3}$	0.028	Kim et al. (2001) and Gobler et al. (2012)
P_k	Half-saturation coefficient for DIP	$g\ P\ m^{-3}$	0.0177	Kim et al. (2001)
θ_R	Constant for quantifying the temperature effect on respiration rate		1.07	Calibrated
OM_{12k}	Half saturation coefficient for organic matter smaller than 12 μm	$g\ C\ m^{-3}$	0.0263	Jeong et al. (2004)
a (a_{1C}, a_{1N}, a_{1P}, a_{2C}, a_{2N}, a_{2P})	Fraction of refractory and labile particulate organic matter smaller than 12 μm, excluding prey algae		0.01	Calibrated
b (b_2, b_3)	Fraction of co-occurring algae that are prey to *M. polykrikoides*		0.001	Derived from observations

Table 3. Sensitivity tests for examining the effects of mixotrophic growth, swimming, and cyst germination on the initiation and development of *M. polykrikoides* blooms. Significant differences between experimental and the Base treatment are shown in bold.

Experiment		***Osmotrophy***	***Phagotrophy***		w_c **(m d^{-1})**	$germ_{ini}$ **(cells m^{-2} d^{-1})**
			a	***b***		
Base		on	0.01	0.001	55	25000
1	Higher bioavailable POM	on	**0.1**	0.001	55	25000
2	Osmotrophy only	on	**0**	**0**	55	25000
3	photoautotrophy only	**off**	**0**	**0**	55	25000
4	Reduced swimming speed	on	0.01	0.001	**30**	25000
5	No swimming	on	0.01	0.001	**0**	25000
6	Higher initial cell loading	on	0.01	0.001	55	**250000**
7	Lower initial cell loading	on	0.01	0.001	55	**2500**

Table 4. The initial time (t_{ini}), when *M. polykrikoides* was first observed in water samples, the date at which *M. polykrikoides* reached bloom densities (t_{bloom}, 1000 cells ml^{-1}), the duration of bloom initiation period (t_B), the duration of the bloom events (density > t_{bloom}), maximum surface cell densities, and mean surface cell densities for each modeled year from 2007-2013 (Base Scenario). Note that the initial time is the same for each station, and only days with a density over 1000 cells ml^{-1} are included for computing duration of the bloom and mean surface cell densities during each bloom.

Year	Station	Initial time (t_{ini})	Beginning of bloom event (t_{bloom})	Duration of initiation period (t_B, d)	Duration of bloom event (weeks)	Maximum surface cell density (cells ml^{-1})	Mean surface cell density during bloom event (cells ml^{-1})
2007	LFB01	6/29/2007	7/15/2007	17	10.4	6335	1052
	NYCC		7/23/2007	25	7.4	6038	735
	LFA01		8/4/2007	37	5.5	4190	742
	LE5.6		8/13/2007	46	3.9	3877	1263
	LE5.4		8/11/2007	44	4.5	4328	925
2008	LFB01	7/1/2008	7/22/2008	22	8.6	8840	1464
	NYCC		8/2/2008	33	6.0	6145	863
	LFA01		8/3/2008	34	5.8	4558	792
	LE5.6		8/13/2008	44	4.1	3915	1230
	LE5.4		8/13/2008	44	4.1	5180	1097
2009	LFB01	5/20/2009	6/26/2009	38	8.8	10290	1662
	NYCC		7/3/2009	45	7.8	6634	1031
	LFA01		7/3/2009	45	7.8	4539	982
	LE5.6		7/9/2009	51	6.9	4436	1180
	LE5.4		7/16/2009	58	5.9	3850	976
2010	LFB01	6/8/2010	7/20/2010	43	9.6	7195	1171
	NYCC		7/19/2010	42	7.9	3050	769
	LFA01		7/19/2010	42	7.3	4978	791
	LE5.6		7/26/2010	49	7.2	4731	1327
	LE5.4		7/29/2010	52	5.6	4849	1154
2011	LFB01	5/27/2011	7/24/2011	59	5.6	1920	584
	NYCC		8/8/2011	74	4.1	4554	708
	LFA01		8/8/2011	74	4.0	6408	813
	LE5.6		8/11/2011	77	3.3	4393	1283
	LE5.4		8/6/2011	72	4.9	4172	1114
2012	LFB01	4/15/2012	6/22/2012	69	12.8	7469	1198
	NYCC		7/3/2012	80	7.1	4640	850
	LFA01		7/1/2012	78	7.2	5824	845
	LE5.6		7/2/2012	79	7.6	2698	982
	LE5.4		7/7/2012	84	7.1	2232	866
2013	LFB01	6/16/2013	7/22/2013	37	9.3	8466	1251
	NYCC		7/25/2013	40	7.0	11666	1199
	LFA01		8/16/2013	62	3.8	10776	1083

LE5.6	8/19/2013	65	3.0	3445	1130
LE5.4	8/24/2013	70	2.0	1936	725

Table 5. The 7-year mean of growth rates, metabolism rate, and transport rate during the modeled blooms in 2007-2013, in units of d^{-1}. We include relative growth rate, $\overline{r_g}$, mixotrophic gross growth rate, $\bar{G}$, phototrophic growth rate, $\overline{G^p}$, heterotrophic growth rate, $\overline{G^h}$, total metabolism rate, $\overline{R}$, and transport rate, $\overline{F_B}$. Values presented are for depth-integrated biomass described in Eq. (8) while the bracket "⟨ ⟩" denotes the mean values over the given periods. Note that *M. polykrikoides* reached bloom densities (1000 cells ml^{-1}) at different times at each station.

Station	**Period**	$\langle\overline{r_g}\rangle$	$\langle\bar{G}\rangle$	$\langle\overline{G^p}\rangle$	$\langle\overline{G^h}\rangle$	$-\langle\bar{R}\rangle$	$-\langle\overline{F_B}\rangle$	$\langle\overline{G^h}\rangle / \langle\bar{G}\rangle$	$\langle\overline{F_B}\rangle / \langle\bar{G}\rangle$
LFB01	Present	0.13	0.18	0.09	0.09	-0.06	0.01	0.51	-0.06
	Initiation	0.39	0.31	0.15	0.16	-0.07	0.15	0.52	-0.48
NYCC	Present	0.18	0.27	0.15	0.12	-0.07	-0.02	0.43	0.08
	Initiation	0.34	0.40	0.22	0.18	-0.08	0.02	0.46	-0.05
LFA01	Present	0.18	0.30	0.17	0.12	-0.07	-0.05	0.42	0.17
	Initiation	0.31	0.42	0.24	0.19	-0.08	-0.03	0.44	0.08
LE5.6	Present	0.19	0.30	0.15	0.14	-0.06	-0.04	0.48	0.14
	Initiation	0.29	0.44	0.22	0.22	-0.07	-0.07	0.49	0.17
LE5.4	Present	0.19	0.34	0.13	0.21	-0.06	-0.10	0.63	0.29
	Initiation	0.28	0.48	0.19	0.29	-0.07	-0.14	0.61	0.28

Footnote: "Present Period": refers to the entire period of time when the cell density of *M. polykrikoides* is greater than 0 cell ml^{-1} in the water column, including both bloom and non-bloom periods; "Initiation Period": refers to the period between the time when the initial cell density was greater than 0 (i.e., t_{ini}) and the time when the density of *M. polykrikoides* reached 1000 cells ml^{-1}, t_{bloom}.

Table 6. The shifts in timing of the beginning of the bloom event, t_{bloom}, (Experiment – Base Scenario) in units of d at two Lafayette River stations, LFB01 and LFA01, due to simulated changes in the fraction of bioavailable particulate organic matter or mixotrophic ability (Exps. 1-3), changes of swimming speed of *M. polykrikoides* (Exps. 4-5), and changes of the magnitude of initial cell loading, $germ_{ini}$ (Exps. 6-7). Positive and negative values indicate that t_{bloom} in the experiments are advanced and delayed, respectively, compared with Base Scenario. The cases when bloom density cannot be reached is denoted by "—".

	Exp. 1	**Exp. 2**	**Exp. 3**	**Exp. 4**	**Exp. 5**	**Exp. 6**	**Exp. 7**
LFB01							
2007	0.0	0.0	0.0	—	—	-2.0	18.2
2008	0.0	0.0	12.0	37.8	45.0	-2.0	11.3
2009	0.0	0.0	54.3	19.5	29.0	-13.0	6.8
2010	0.0	0.0	—	5.3	22.8	-2.0	4.3
2011	0.0	0.0	—	21.8	34.3	-7.2	37.8
2012	-0.8	0.0	—	56.0	35.5	-8.5	14.2
2013	0.0	0.0	—	35.5	—	-11.8	2.8
LFA01							
2007	-1.3	0.0	—	—	—	-12.5	12.2
2008	0.0	0.0	—	29.8	—	-2.3	5.8
2009	0.0	0.0	—	11.5	39.7	-10.5	7.5
2010	0.0	0.0	—	6.5	—	-2.0	10.0
2011	-15.3	0.0	—	0.3	21.5	-29.5	13.3
2012	0.0	0.0	—	45.5	—	-15.2	10.8
2013	0.0	0.0	—	9.0	—	-22.8	4.0

Table 7. The 7-year mean of the modeled daily-averaged growth-limiting function for each environmental factor, including temperature (T), salinity (Sal), irradiance (I), dissolved inorganic nitrogen (DIN), dissolved inorganic phosphate (DIP), and bioavailable organic matter that is smaller than 12 μm (OM_{12}), during the simulated blooms in 2007-2013. The mean of $f(Res)$ that represents the overall contribution of resources (I, DIN, DIP, and OM_{12}) is also presented. Note that the values are for the surface layer only, $f(I)$ equals zero at night and the means for $f(I)$ during the photic period between 6:00 to 18:00 are listed in parentheses.

Station	**Period**	$f(T)$	$f(Sal)$	$f(Res)$	$f(I)$	$f(DIN)$	$f(DIP)$	$f(OM_{12})$
LFB01	Present	0.59	0.48	0.82	0.53 (0.97)	0.40	0.70	0.74
	Initiation	0.64	0.46	0.97	0.54 (0.97)	0.55	0.68	0.95
NYCC	Present	0.72	0.54	0.85	0.53 (0.97)	0.60	0.58	0.70
	Initiation	0.73	0.51	0.98	0.54 (0.98)	0.72	0.58	0.91
LFA01	Present	0.76	0.55	0.86	0.53 (0.97)	0.65	0.57	0.71
	Initiation	0.76	0.52	0.97	0.54 (0.97)	0.75	0.58	0.91
LE5.6	Present	0.82	0.56	0.84	0.53 (0.97)	0.66	0.56	0.70
	Initiation	0.82	0.54	0.97	0.54 (0.97)	0.77	0.58	0.90
LE5.4	Present	0.87	0.61	0.89	0.53 (0.97)	0.60	0.53	0.80
	Initiation	0.87	0.59	0.98	0.53 (0.97)	0.72	0.53	0.92

Footnote: "Present Period": refers to the entire period of time when the cell density of *M. polykrikoides* is greater than 0 cell ml^{-1} in the water column, including both bloom and non-bloom periods; "Initiation Period": refers to the period between the time when initial density was larger than 0 (i.e., t_{ini}) and the time when the density of *M. polykrikoides* reached 1000 cells ml^{-1}, t_{bloom}.

Table 8. r^2 between the modeled gross growth rate, G, and the modeled daily-averaged growth-limiting function for temperature (T), salinity (Sal), and $f(Res)$ that represents the overall contribution of resources (I, DIN, DIP, and OM_{12}) to the variability in G; and r^2 between $f(Res)$ and daily-averaged growth-limiting function for irradiance (I), dissolved inorganic nitrogen (DIN), dissolved inorganic phosphate (DIP), and organic matter smaller than 12 μm (OM_{12}). Statistics are reported for interannual variability and daily variability, respectively for the modeled 7-year dataset encompassing the years 2007-2013. Note that the values are for the surface layer only and that *M. polykrikoides* cell abundances at each station reached bloom densities at different times. Significant values with p-values less than 0.05 are shown in bold.

Station	**Period**	$\boldsymbol{f(T)\sim G}$	$\boldsymbol{f(Sal)\sim G}$	$\boldsymbol{f(Res)\sim G}$	$\boldsymbol{f(I)\sim f(Res)}$	$\boldsymbol{f(DIN)\sim f(Res)}$	$\boldsymbol{f(DIP)\sim f(Res)}$	$\boldsymbol{f(OM_{12})\sim f(Res)}$
Interannual								
LFB01	Present	**0.67**	0.07	0.02	0.14	0.46	<0.01	**0.98**
	Initiation	**0.95**	0.03	0.01	0.55	**0.58**	0.32	0.13
NYCC	Present	**0.75**	0.08	0.31	0.18	**0.65**	0.01	**0.91**
	Initiation	**0.77**	<0.01	0.43	0.09	0.13	0.34	0.03
LFA01	Present	**0.69**	0.03	0.48	0.20	**0.71**	0.02	**0.87**
	Initiation	**0.61**	<0.01	0.51	0.01	0.31	0.08	0.03
LE5.6	Present	**0.66**	0.06	0.42	0.21	**0.78**	0.04	**0.88**
	Initiation	0.39	0.02	0.16	0.40	0.02	0.20	0.01
LE5.4	Present	0.56	<0.01	0.23	0.18	**0.73**	<0.01	**0.88**
	Initiation	0.54	0.05	0.04	0.26	0.05	0.34	0.09
Daily								
LFB01	Present	**0.42**	**0.04**	**0.22**	**0.22**	**0.30**	**0.01**	**0.96**
	Initiation	**0.94**	**0.02**	**0.02**	**0.07**	**0.10**	**0.02**	<0.01
NYCC	Present	**0.42**	**0.07**	**0.29**	**0.33**	**0.50**	<0.01	**0.93**
	Initiation	**0.89**	0.01	**0.03**	<0.01	**0.03**	<0.01	<0.01
LFA01	Present	**0.40**	**0.05**	**0.31**	**0.32**	**0.55**	**0.01**	**0.92**
	Initiation	**0.82**	**0.01**	**0.06**	<0.01	**0.10**	<0.01	<0.01
LE5.6	Present	**0.25**	**0.06**	**0.47**	**0.33**	**0.72**	**0.04**	**0.93**
	Initiation	**0.75**	**0.01**	**0.05**	**0.04**	**0.03**	**0.01**	**0.36**
LE5.4	Present	**0.33**	<0.01	**0.36**	**0.25**	**0.60**	**0.01**	**0.90**
	Initiation	**0.76**	**0.04**	**0.05**	<0.01	**0.01**	<0.01	**0.09**

Footnote: "Present Period": refers to the entire period of time when the cell density of *M. polykrikoides* is greater than 0 cell ml^{-1} in the water column, including both bloom and non-bloom periods; "Initiation Period": refers to the period between the time when initial density was larger than 0 (i.e., t_{ini}) and the time when the density of *M. polykrikoides* reached 1000 cells ml^{-1}, t_{bloom}.

Figure Captions

Figure 1. Map of the lower James River and the Elizabeth and Lafayette River sub-tributaries, Virginia, USA. The hollow squares denote the locations of long-term monitoring stations LE5.4 (polyhaline James River), LE5.6 (lower Elizabeth River), LFA01 (Lafayette River mouth), and LFB01 (Lafayette River headwaters), and the filled circle denotes the location of Station NYCC.

Figure 2. Comparison of modeled daily surface chl-a from 2007-2013 at monitoring stations in the Lafayette River (LFB01, NYCC, and LFA01), the Elizabeth River (LE5.6), and the mainstem James River (LE5.4). The blue area represents the area between the minimum and the maximum chl-a, the monthly chl-a data from the Chesapeake Bay Program data are indicated by the dots and the weekly dataflow chl-a data are indicated by the diamonds. The correlation coefficients (r) between the model output and observational data of surface chl-a at the five stations and the relative errors (RE) are listed. The grey area represents the initiation periods that are bounded by the time of initial cell loading, t_{ini}, and the time when bloom cell densities were reached, t_{bloom}.

Figure 3. Comparison of model results of *M. polykrikoides* cell densities at station LFB01 (Base Scenario) to the observational density data (red circles) in the Lafayette River in 2009. The thick blue line is the daily-averaged modeled *M. polykrikoides* cell density, and the blue area represents the area bounded by the daily minimum and the daily maximum of the modeled cell density in the grid cell representing the station, and the black dashed line indicates the cell density considered to be a bloom (e.g., 1000 cells ml^{-1}).

Figure 4. Daily maximum surface cell densities of *M. polykrikoides* at Station LFB01 during 2009 for each experiment compared with the Base Scenario (black lines), resulting from (A) different fractions of bioavailable particulate organic matter or different mixotrophic capability; Base: a = 0.01, b = 0.001; Exp. 1: a = 0.1, b = 0.001; Exp. 2: osmotrophy only (a = b = 0); Exp. 3: photoautotrophy only (heterotrophy off); (B) different swimming speeds, w_c, Base: w_c = 55 m d^{-1}, Exp. 4: w_c = 30 m d^{-1}, Exp. 5: w_c = 0 m d^{-1}; and (C) different magnitudes of initial cell loadings, $germ_{ini}$; Base: $germ_{ini}$ = 25,000 cells m^{-2} d^{-1}, Exp. 6: $germ_{ini}$ = 250,000 cells m^{-2} d^{-1}, Exp. 7: $germ_{ini}$ = 2,500 cells m^{-2} d^{-1}. The red dotted lines indicate the time when bloom cell densities were reached in Base Scenario, t_{bloom}.

Figure 5. The daily-averaged gross growth rate, G, phototrophic growth rate, G^p, heterotrophic growth rate, G^h, growth-limiting functions for temperature, $f(T)$, salinity, $f(Sal)$, irradiance, $f(I)$, dissolved inorganic nitrogen, $f(DIN)$, dissolved inorganic phosphate, $f(DIP)$, and organic matter smaller than 12 μm, $f(OM_{12})$, at Station LFB01 in 2012 (left panels) and 2013 (right panels). G_{TS} is also plotted, $G_{TS} = G_{opt} f(T) f(Sal)$, which is the highest potential

growth rate based on temperature and salinity limitation (i.e., other resources are not limited). The initiation periods are bounded by the black dotted lines indicating the time of initial cell loading, t_{ini}, and the red dotted lines indicate the time when bloom cell densities were reached, t_{bloom}.

Chesapeake Bay
James River
Chesapeake
Atlantic Ocean
LE5.4
LFA01
NYCC
LE5.6
LFB01
Lafayette R.
Elizabeth R.
N
0 2.5 5 10 km
37°0'N
76°30'W
76°15'W

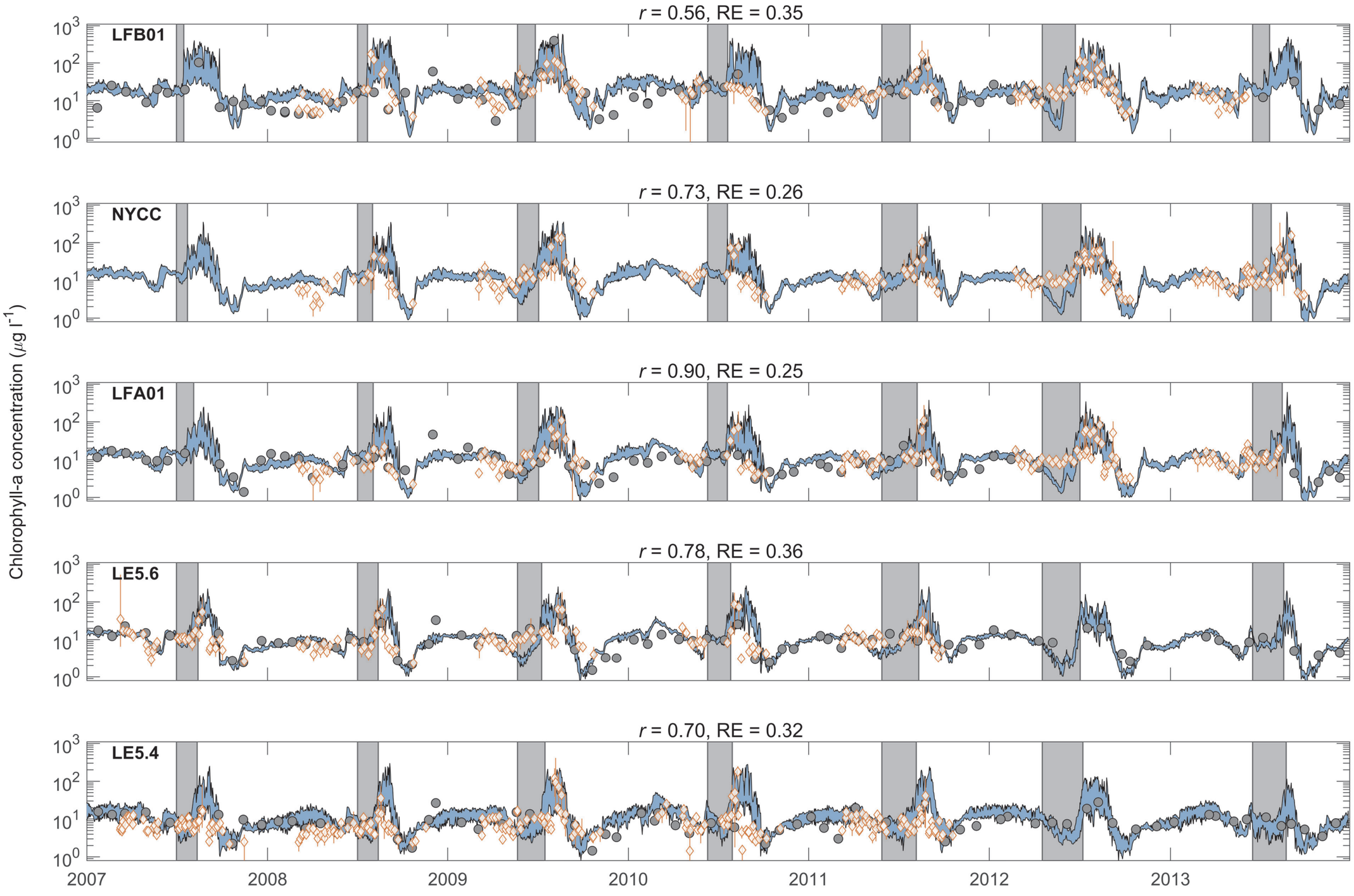
r = 0.56, RE = 0.35
LFB01
r = 0.73, RE = 0.26
NYCC
r = 0.90, RE = 0.25
LFA01
r = 0.78, RE = 0.36
LE5.6
r = 0.70, RE = 0.32
LE5.4
Chlorophyll-a concentration (μg l-1)
10^3
10^2
10^1
10^0
2007
2008
2009
2010
2011
2012
2013

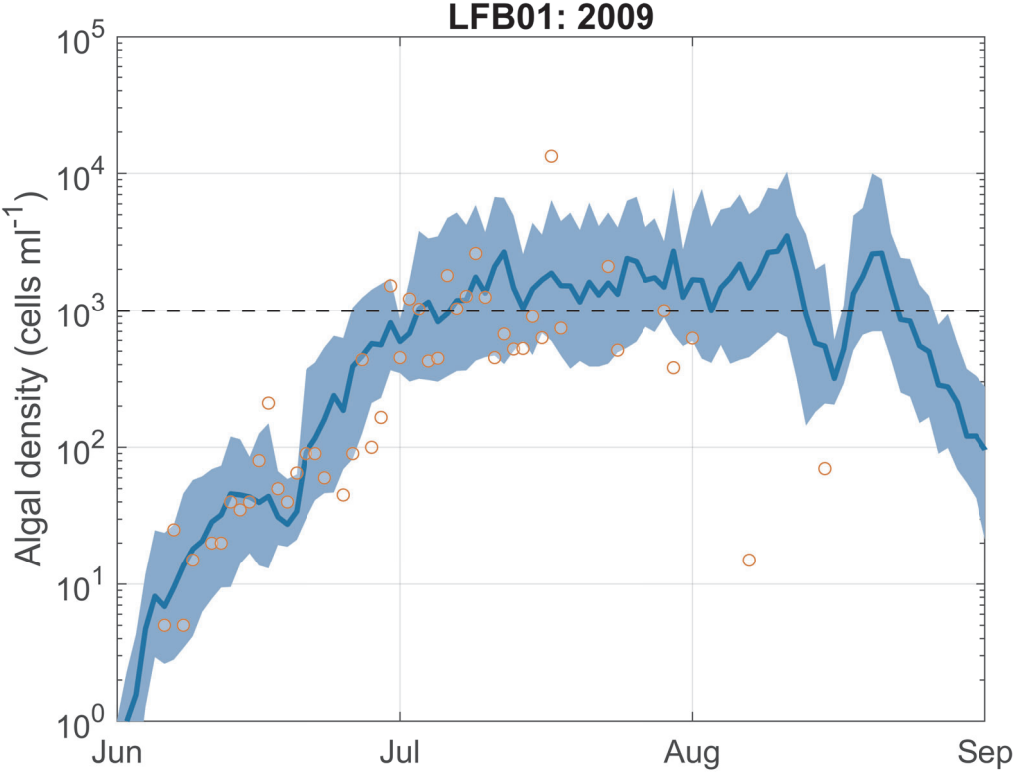
LFB01: 2009
Algal density (cells ml-1)
10^5
10^4
10^3
10^2
10^1
10^0
Jun
Jul
Aug
Sep

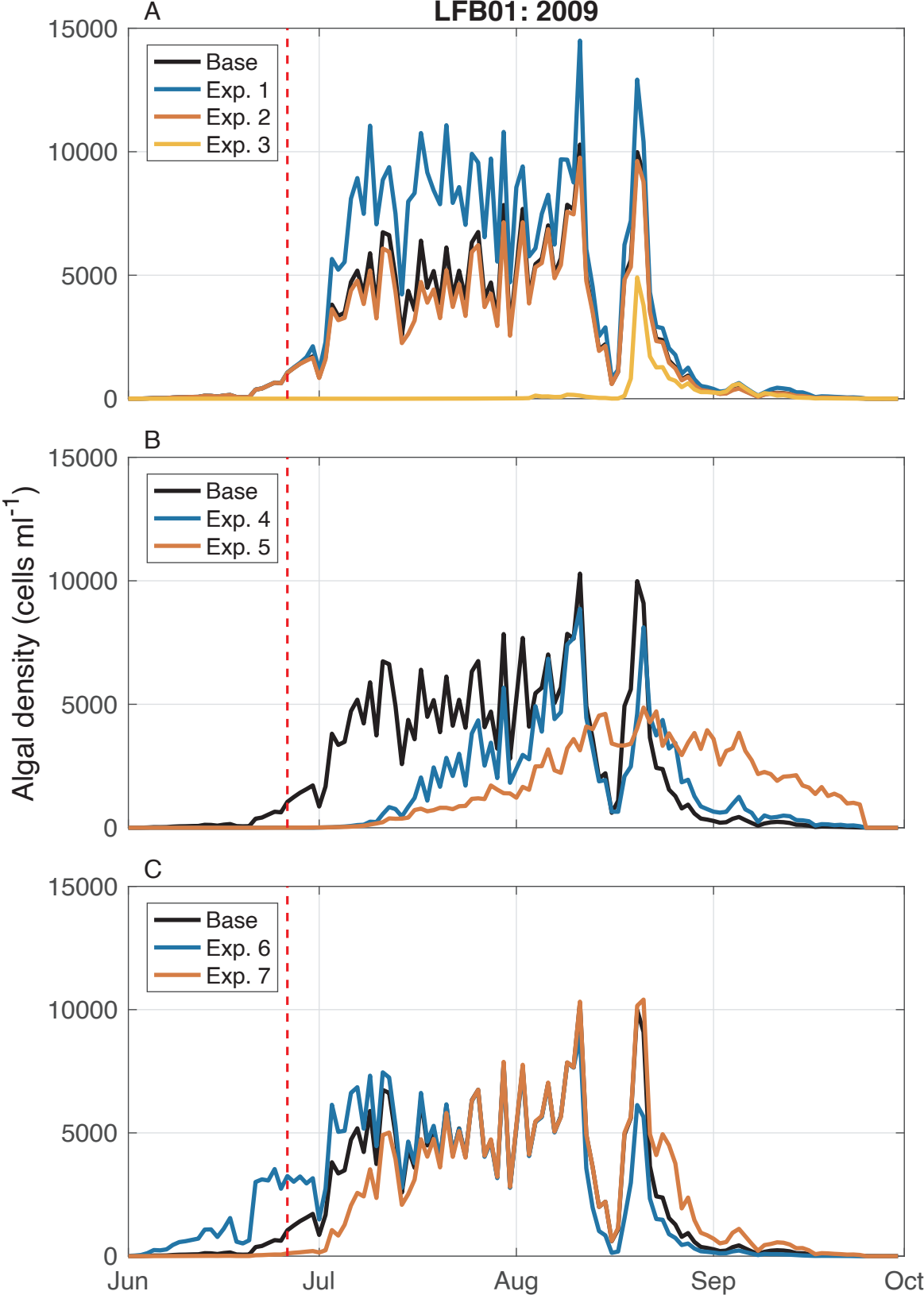
LFB01: 2009
A
B
C
Base
Exp. 1
Exp. 2
Exp. 3
Exp. 4
Exp. 5
Exp. 6
Exp. 7
15000
10000
5000
0
Algal density (cells ml-1)
Jun
Jul
Aug
Sep
Oct

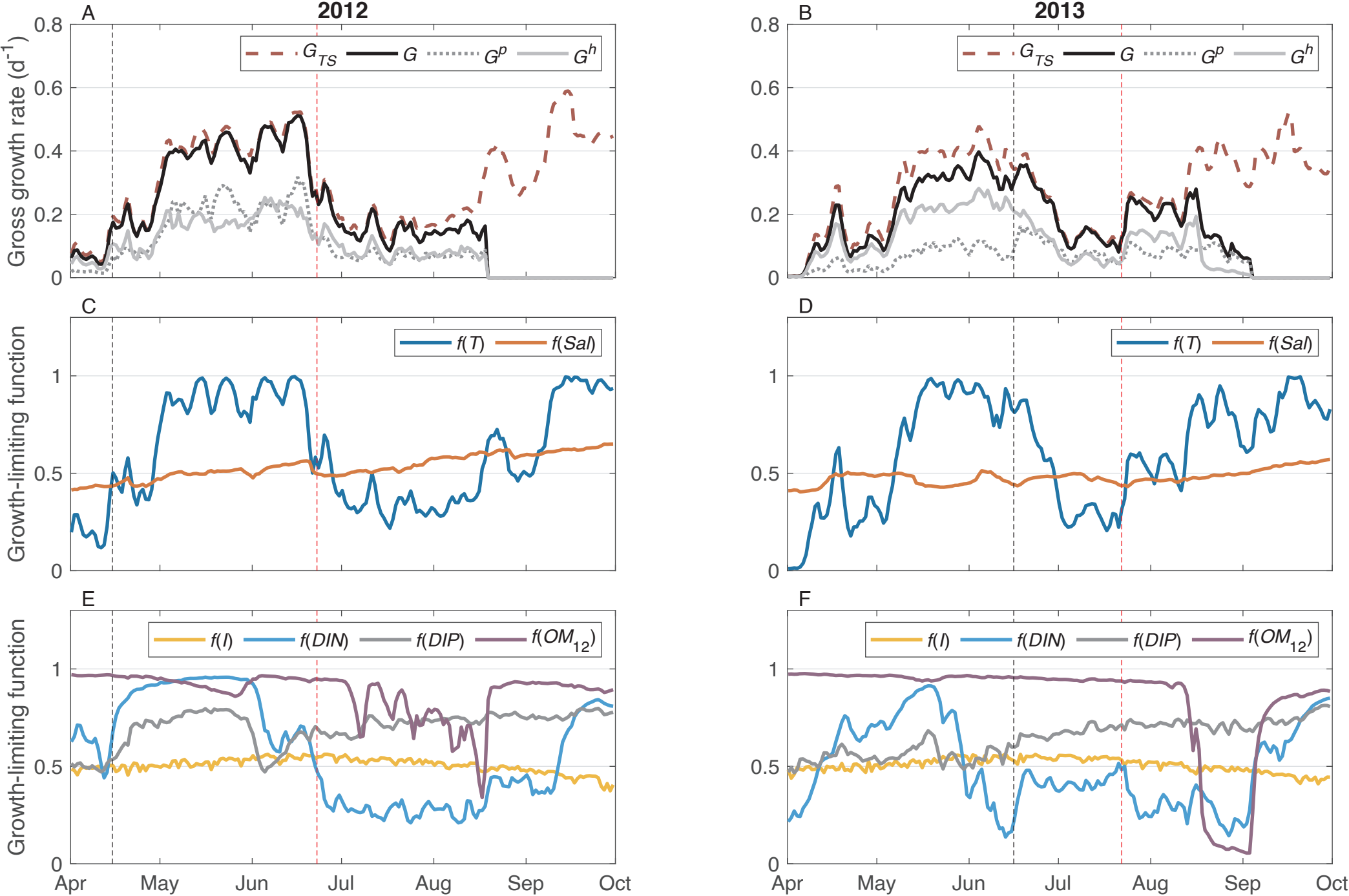
A
2012
B
2013
C
D
E
F
Gross growth rate (d-1)
Growth-limiting function
Growth-limiting function
GTS
G
Gp
Gh
f(T)
f(Sal)
f(I)
f(DIN)
f(DIP)
f(OM12)
0
0.2
0.4
0.6
0.8
0.5
1
Apr
May
Jun
Jul
Aug
Sep
Oct